Catheter Based Magnetic Resonance Compatible Perfusion Probe
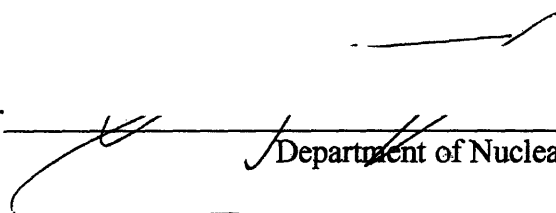
by

Cara Lynne Toretta

Submitted to the Department of Nuclear Science and Engineering
in Partial Fulfillment of the Requirements for the Degrees of Bachelor of Science and
Master of Science in Nuclear Science and Engineering

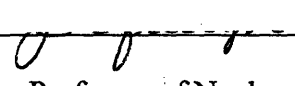at the

Massachusetts Institute of Technology
February 2007

Signature of Author_____
Department of Nuclear Science and Engineering
January 31, 2007
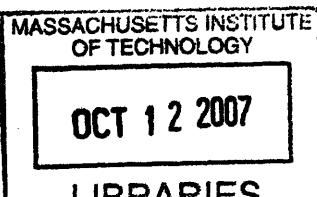
Certified by_____
Dr. H. Frederick Bowman
Senior Academic Administrator
Thesis Supervisor

Certified by_____
Dr. Jacquelyn C. Yanch
Professor of Nuclear Science and Engineering
Thesis Reader

Accepted by_____
Dr. Jeffrey A. Coderre
Department of Nuclear Science and Engineering
Chairman, Department Committee on Graduate Students

- 1 -

Catheter Based Magnetic Resonance Compatible Perfusion Probe

by

Cara Lynne Toretta

Submitted to the Department of Nuclear Science and Engineering
on January 31, 2007 in Partial Fulfillment of the Requirements
for the Degrees of Bachelor of Science and Master of Science
in Nuclear Science and Engineering

Abstract:

Neurosurgeons are using a thermal based technique to quantify brain perfusion. The thermal diffusion probe (TDP) technology measures perfusion in a relatively small volume of brain tissue. The neurosurgeon chooses the specific brain location and probe placement based on their clinical concern. When an early indication of compromised perfusion is detected by the TDP, it is generally necessary to confirm the local, absolute perfusion measurement taken with the TDP, with magnetic resonance (MR) perfusion imaging. MR perfusion imaging provides an excellent, but relative, global assessment of compromised tissue perfusion. Due to the many clinical and diagnostic benefits of real-time, absolute quantification of blood flow acquired by the TDP, there has been increased interest in having the TDP MR compatible. This thesis considers what it would take to render the TDP MR compatible in both the active and passive modes. The analysis considers effects of the EM field on the probe, and the probe on the MR image. The presence of cardiac and respiratory induced brain motion has been shown to provide an artifact in TDP perfusion data. Consideration is given to ways in which to minimize this motion induced perfusion artifact.

Thesis Supervisor: Dr. H. Frederick Bowman
Title: Senior Academic Administrator

Thesis Reader: Dr. Jacquelyn C. Yanch
Title: Professor of Nuclear Science and Engineering

Table of Contents   **Page**

List of Figures

Chapter 1 – Introduction

This project deals with the quantification of perfusion in brain tissue using the Thermal Diffusion Probe (TDP). The TDP provides local, real-time, continuous, and absolute values of perfusion. The TDP is currently used in neurosurgery by early adopters to monitor the level of brain perfusion (blood flow) during traumatic brain injury (TBI) and in those patients at risk for vasospasm subsequent to subarachnoid hemorrhage. The two major foci of this thesis are: 1) consideration of what it would take to render the TDP sensor probe MR compatible; and 2) consideration of cardiac induced brain tissue motion and the impact of that motion on the accuracy of TDP derived perfusion values.

Early indications of compromised brain perfusion detected regionally by the TDP are routinely confirmed by global CT-angiograms or MR perfusion scans. Currently, the non-MR compatible TDP sensor has to be removed from the patient before the MR scan is conducted. Probe removal eliminates the acquisition of continuous perfusion data before, during, and after the scan. Following the MR scan, the clinician has to either forego post scan absolute monitoring or must insert a new TDP probe, which is costly. Furthermore, placement of a second probe risks the probe being situated in a different location. This makes pre vs. post perfusion values a bit more complex to evaluate due to brain tissue flow heterogeneity. CT-angiograms and MR perfusion scans allow for global, though relative, analysis of compromised perfusion, while the TDP provides a local, though absolute, assessment of perfusion. Absolute perfusion values are extremely important for overall patient assessment. For example, if the flow in the human brain is

less than 15 ml/100g*min, the patient begins to lose brain function and if it is less than 7 ml/100g*min, the brain tissue begins to lose viability. Having a local /regional, but absolute measure of tissue perfusion improves patient diagnosis, early detection of ischemia and subsequent clinical management. While local/regional measures are valuable in identifying perfusion problems; global 3D perfusion assessment via CT-angiograms or MR perfusion scans are necessary to detect the extent of the problem. For these complementary reasons, clinicians have expressed interest in a TDP sensors which does not need to be removed during MR scans. This thesis considers what would be required to take MR scans with the TDP in place while operating in both active and passive modes.

Pulsatile flow components have recently been observed in brain perfusion data taken by the TDP that seems to match the frequencies associated with heart and respiration rates. This pulsatile flow component derives from a periodic motion artifact and may artificially elevate the measured perfusion levels. Cardiac and respiratory induced brain tissue motion gives rise to periodic relative probe-tissue motion, which causes a periodic increase in power-time relationship, which often leads to an artificially elevated perfusion value. To remove or reduce this motion artifact, the motion frequency, direction, and amplitude have to be known and quantified. An appropriate thermal model may then be developed and incorporated into the perfusion extraction algorithm to remove the effect of the motion artifact. Alternatively, one might design an appropriate probe insertion/implantation technique that effectively avoids the motion.

In conclusion, in addition to addressing what would render the TDP MR compatible, the work reported in this thesis seeks to identify the source(s), and to characterize the cardiac and respiratory induced brain motion that is present and which in turn influences the TDP power-time data. Once characterized, models, which are beyond the scope of this thesis, can be developed to isolate and remove the motion effects or positioning techniques may be conceived which will minimize the resulting relative probe-tissue motion and its associated artifact.

Chapter 2 - Perfusion

2.1 Functional Anatomy

The cardiovascular system regulates blood flow. The main function of the cardiovascular system is to deliver nutrient carrying blood to the tissues while concurrently removing waste. The heart pumps the blood around the body through a closed system of blood vessels. The arteries carry blood away from the heart and are under higher pressure than the veins, which carry blood back to the heart. Arteries, or more accurately the pre-capillary arterioles feed the capillaries which have very thin walls that allow for the exchange of materials down their concentration gradient via diffusion. There is an exchange of oxygen, nutrients, waste, heat, and fluid across the capillary walls. Blood from the capillaries is collected by the venous system and returned to the heart. The cardiovascular system is also involved in the regulation of body temperature, blood pressure, and homeostasis.

The rate of blood flow, cardiac output, in the body operates in steady state, meaning that the rate of blood flow leaving the right ventricle (to the lungs) equals the rate of blood leaving the left ventricle (to the body). Once the blood leaves the heart, certain percentages of the cardiac output go to each of the physiological systems. This results in variable blood flow between the organs in the body depending on local demand and vascular resistance. Blood flowing through specific vessels is dependant on the resistance of the blood vessel, and the pressure gradient between the ends of the vessel.

The flow relationship is comparable to that of an electrical circuit. Ohm's law states that $I = \Delta V/R$, where the current is I, the voltage is V, and the resistance is R. Blood flow is similar to current flow, pressure gradient is similar to voltage gradient, and the vascular resistance is similar to electrical resistance. This leads to the equation: $Q = \Delta P/R$. Where Q is the flow (ml/min), ΔP is the pressure difference (mmHg), and R is the resistance (mmHg/ml/min). [15]

This equation shows that the blood flow is inversely proportional to the resistance. Thus, if the vascular resistance decreases, the flow increases. Changing the resistance of a blood vessel is the chief means for changing blood flow within the cardiovascular system. Due to the strength of the walls of the arteries, this resistance change typically occurs in the pre-capillary arterioles which directly affect the flow to the capillaries. Considering that the cardiac output is in steady state, this puts the resistance of each physiological system in parallel. Where the overall resistance of the body is less than the individual resistances, this means that there is minimal loss of pressure in the major arteries. Within a physiological system, the resistance is in series, where the total resistance of the system is equal to the sum of the individual resistances. This makes the flow through each class of vessels the same within the organ, and causes the pressure to decrease progressively with the arterioles having the highest pressure gradient, $\Delta P = Q \times R$. [15]

Specific resistance is unique to each organ. Every organ has its own metabolic demand that determines the blood flow requirement which is established by regulating internal resistance. If part of an organ is in a compromised state, the resistance can change

allowing for more blood to flow to that area. Resistance of the vessels in the cardiovascular system thus maintains the distribution of blood flow throughout the body. Specific vascular resistance in normal physiology directly relates to the amount of blood that is needed to keep the tissue in a normal, functional state. Every tissue has an optimal level of perfusion. Perfusion is defined as the rate of blood flow in tissue per unit mass. The units are milliliters of blood per 100 grams per minute, or ml/100g*min. As blood perfusion decreases from the optimal level, then there is an increased probability of loss of tissue function and ultimately tissue death.

It is essential for tissue survival and function that such compromised states are discovered and resolved in a timely manner. Rapid reversal of compromised states offers a better prognosis for tissue revival. Thus, the quantification of tissue perfusion is a long sought after capability with extensive clinical applications. Perfusion measurements are extremely important in both the assessment and management of an injury or trauma.

2.2 Various Methods of Measuring Perfusion

Since the beginning of medical imaging there has been quite a few techniques used for measuring perfusion. They can be classified in two distinct categories corresponding to the tracer methods: exogenous tracer method and endogenous tracer method. [2] [3] An exogenous tracer is one that is isolated to the intravascular compartment, i.e. inside the blood vessel, and does not diffuse to the extracellular space. Endogenous, on the other

hand, is not restricted to the intravascular compartment and does diffuse freely to the extracellular space.

2.2.1 Diffusible Tracer

The diffusible tracer method relates the amount of tracer allotted to the patient, to the relative amount that is taken up by the tissue. A tracer is used to selectively sample the tracer's concentration or to record the emission from the tracer. One example of a diffusible tracer is Xenon-Enhanced CT. Xenon-CT has been a widespread technique used for many year. [3] Xenon is a very small molecule that is both water and lipid soluble and it moves freely after being inhaled and then dissolved in the blood. The concentration of the Xe gas reflects the input and uptake of Xe by the tissue. Due to the perfusion dependent washout attenuation of Xenon, it makes it a very good contrast agent and can be easily imaged through x-ray sensitive CT scanning.

Another widely used diffusive technique is single photon emission CT or SPECT. [3] This technique is based on the diffusion of the radioisotope technitium-99m (Tc-99m). The radioisotope is attached to a compound that can diffuse into the cells and is metabolized by neuronal and glial cells. On its first pass, most of the Tc-99m will attach to the respective cells and the uptake is proportional to the blood flow. The concentration distribution of the Tc-99m can be used to represent the distributed relative blood flow at the time of application.

The non-diffusible tracer techniques are used more often, and provide a more reliable

method for perfusion imaging. [3] CT offers a very reliable way to measure perfusion

with an endogenous tracer. It measures the changes of tissue density following an

injection of a contrast agent that stays within the vascular space. With that assumption,

very fast image slices are taken over a limited volume to determine density changes over

time, arterial input, and venous outflow values. These are then put into a mathematical

algorithm that calculates blood volume, flow, and transit time.

2.2.2 MR Perfusion Techniques

A technique that presents great promise for the future is MR perfusion imaging. MR

imaging is a commonly used method that makes use of the natural magnetization of tissue

to create an image. Magnetic resonance imaging is a very attractive technique because it

offers the most accurate and highest resolution image, and does not use ionizing

radiation. [2]

Before MR perfusion is discussed, a basic foundation of MR imaging must be

established. [4] [5] A more detailed explanation of Nuclear Magnetic Resonance (NMR)

information will be presented in Chapter 3. For the sake of understanding MR perfusion

techniques, a summary will follow. There are many factors that pertain to the quality of

the image, such as signal to noise ratio (SNR), spatial resolution, and tissue contrast.

Spatial resolution and tissue contrast are determined by the parameters of the examination

and the area being imaged. Each organ has certain properties that pertain to certain parameters in an examination.

There is a critical SNR threshold above which MR images have clear resolution of the organs being imaged. Each of the three factors (SNR, spatial resolution, and tissue contrast) is largely dependent on intrinsic (tissue dependent) and extrinsic (operator-dependent) parameters. The most important intrinsic parameters are proton density and the magnetic relaxation time. These correspond to T1 and T2. Extrinsic parameters include magnetic field strength, repetition time (TR), echo time (TE), matrix size, slice thickness, field of view, number of data acquisitions, radiofrequency coils, and other factors. Most important for MR perfusion imaging are the intrinsic parameters and their direct affect on TR and TE.

The intrinsic properties of the sample T1 and T2 determines the quality of the image resolution. They will determine the repetition time and the echo time of the operator. T1 refers to the time needed for the recovery of a longitudinal magnetization along the z axis to return to its equilibrium value following a 90 degree pulse. T1 is the longitudinal relaxation time and is also called the spin-lattice relaxation time because it depends on the nuclei losing energy to the surrounding environment. Tissues with a short T1 return to their magnetization equilibrium at a faster rate than tissues with a long T1. Therefore T1 determines when the next RF pulse can be applied. If it is applied before T1, there will be a reduction in the free induction decay. The free induction decay is the basic MR signal that occurs as an exponentially decaying oscillation of signal amplitude as a

function of time. Consequently, the differences in T1 relaxation of various tissues can be exaggerated by altering the time between RF pulses. If the time between 90 degree pulses is short, i.e. a short TR, then the differences in tissues with different T1 values will be emphasized. Those tissues with a short T1 will be able to get closer to equilibrium before the next pulse and will not have a reduction in the free induction decay. Therefore the tissue with lower T1 will appear at a higher signal frequency. [4] If the opposite occurs, where TR is long then all tissue T1 values will be able to get back to equilibrium and there will be little contrast between the tissues. This is the basis of T1 weighted imaging.

The other intrinsic relaxation T2, is net loss of magnetization in the transverse plane due to dephasing. [4] [5] With an RF pulse, all protons align in phase. Due to slight differences in local magnetic field environments experienced by each proton, the individual precession frequency is slightly different. This is called transverse relaxation and is also often called spin-spin relaxation because it corresponds to interactions between neighboring spinning nuclei. T2 is always less than T1. To emphasize differences in T2, the RF pulses applied to the external magnetic field are changed, this technique is called spin echo. Thus, T2 determines the spin echo or ER.

Spin echo is a serious of RF pulses that correspond to a certain sequence that will provide the best image resolution for the corresponding tissue. Usually the sequence is a 90 degree pulse followed by a 180 degree pulse. [4] Knowing T1, T2, the corresponding echo pulse sequence certain images can be made that are either T1 or T2 weighted.

2.2.3 DSC and ASL Techniques

There are two main types of MR perfusion techniques: one is the first pass bolus tracking technique also known as dynamic susceptibility contrast (DSC), and the other is arterial spin labeling (ASL). [2] ASL is a method that saturates and inverts water protons electromagnetically. The inverted protons mix with the non inverted protons in the blood. Imaging before and after the spin inversion detects tissue magnetization, which is proportional to perfusion. This method is still in its experimental stages and although promising does produce high signal to noise and long acquisition times.

DSC, the more commonly used MR perfusion technique, uses a paramagnetic contrast agent that dephases the protons in the area surrounding the capillary network. This dephasing causes an alternation in the T2 relaxation in the adjacent tissue. There is a temporary change in the local magnetic field surrounding the perfused tissue caused by a bolus of paramagnetic tracer. The change in magnetic field is recorded as the signal changes. Using ultra fast imaging techniques in succession, yields an accurate measurement of the quickly varying signals. The signal variation corresponds to the degree of T2 change which is ultimately proportionate to the perfusion.

The relative tracer concentrations can be analyzed on a time scale that corresponds to the signal-time data. These tracer curves represent the tissue parameters that reflect the blood volume, blood flow, and transit time. The blood volume means the volume of

blood in a given region of tissue and measured in mL/100g of tissue. Blood flow is the volume of blood passing through a given region in a certain time. It is measured in mL/100g/min. The mean transit time, MTT, is the average time it takes blood to pass through a given region of tissue. [2]

Quantitatively these parameters are determined from the graphs of tracer concentration-time data. The arterial input function is deconvolved to get the clearance or mean transit time through the capillary bed. Blood volume is calculated by integrating the area under the deconvolved tissue-concentration time curve and divided by the mean transit time. This gives total concentration in the tissue per time. The initial height of the tissue concentration-time curve can be taken as the blood flow, and the mean transit time can therefore be calculated as the ratio of blood volume to blood flow.

The tissue parameters (blood volume, blood flow, and transit time) are dependent on many factors: patient specific physiological factors and the specifics of the experiment. The parameters are strongly dependent on the bolus arrival time, and thus the amount and paramagnetic properties of the injection. These parameters are also dependent on the person and their cardiac output and their total-body volume. Therefore, no set standard exists for all patients, and only a relative scale can be used that compares the vast variations in the images. It has proven difficult to quantify this technique. There have been a few methods that have tried to quantify the results, but no reliable method has been installed permanently. The image, and the corresponding tissue parameters, give a reliable relative perfusion output.

Endogenous tracers provide another MR perfusion imaging method. [2] [3] The

endogenous, or diffusible, tracer technique measures the regional uptake of a tracer that

has diffused into the tissue compartment and is not limited to the intravascular space.

This method depends on the detection of signal loss from the water protons that flow

within the blood. The water protons are magnetically labeled by the application of a

specific radiofrequency pulse that saturates and inverts them electromagnetically.

Imaging before and after the inversion will detect the differences in tissue magnetization

and give a qualitative or quantitative result.

This newer method still has many unresolved disadvantages and inaccuracies, many

arising from the difficulty of keeping the spins labeled in a certain selected slice. The

protons on the edges of the slice transfer their magnetization to the ones that are not

selected causing an off resonance radio frequency that will cause a huge loss in the

observed signal. The other main loss in this method is due to T1 relaxation from blood

flow from the labeled plane to the imaging plane.

There are methods to counteract these problems. They require longer acquisition times

and are very sensitive to any motion. This method does hold much promise, as a

quantitative result can be obtained in theory. A quantitative result would be very

important for an accurate analysis of an infarction, or tissue death, or ischemia, decreased

flow. A quantitative measure of relative ischemia could provide information on the

possibility of reviving the tissue and the associated physiological problems. Through more clinical trials hopefully this method will be the future for MR perfusion imaging.

Dynamic sequencing can be done with either a T1 or T2 weighted imaging technique. The T2 weighted sequence is more often used in practice. Injection of a paramagnetic contrast agent causes a transient drop in signal intensity. These techniques are T2 (spin echo) or T2* (gradient echo) weighted. T2 weighted has the advantage of decreasing artifact at the tissue-bone and tissue-air interface and is more sensitive to smaller changes especially at the capillary level. The method does, however, require much more contrast agent than the gradient echo. Both T2 and T2* have short imaging times and has the option of multiple slice selection imaging.

T1 weighted imaging does offer better spatial resolution and a lower dose of contrast material. [2] This method measures the reduction of the T1 relaxation time, which results in a higher output on T1 weighted images. This is in contrast to the susceptibility effects of the contrast agent in T2 and T2*. In that technique, the reduction of T2 and T2* relaxation times will lead to a lower signal on T2 and T2* weighted images. Combining both methods will provide a more accurate diagnosis.

2.2.4 Other Techniques

Diffusion MR perfusion imaging is another technique, much like the labeling of water protons, that takes advantage of the waters molecules ability to diffuse. [3] [2] This

ability is evaluated using a strong gradient coil that can provide rapid 180-degree excitation. The random motion of the water molecules diffusing causes a phase shift and a signal loss. Conversely, where there is no diffusion, there will be no loss in regard to a phase shift and a very strong signal. Where there is decreased perfusion there will be less diffusion. This method is also not quantitative but relative using signal strengths to record and obtain diffusion coefficients. A problem arises in the analysis of similar results, because a decrease of signal is observed when the water hits a membrane or large molecule. Instead of looking at diffusion weighted imaging alone, it is often coupled with perfusion weighted imaging. Both these imaging modes combined offer a much better analysis.

Combining perfusion and diffusion weighted imaging will allow for a better assessment of relative reversible or irreversible ischemia. [3] [2] Having information from both types of images can offer information about whether or not the tissue can be revived. Typically if there is decreased perfusion, the diffusion will equilibrate with this decreased value. Thus, if an area has a low perfusion weighted image, but has a normal diffusion weighted image it could mean that the tissue has a potentially reversible ischemia. If the values are the same then chances are the tissue is irreversibly damaged. The method of combining perfusion and diffusion weighted images is still under clinical investigation; where preclinical experiments offer positive results.

A hindrance to accurate perfusion measurements is found in the innate properties of the blood itself. The blood oxygenation level provides a local magnetic field that will alter

the signal near the local blood vessels. [6] The alteration is due to the deoxyhemoglobin acting as an endogenous paramagnetic contrast agent. This affect is called Blood Oxygenation Level-Dependent contrast or BOLD contrast. When there is an increase in local neuronal activity, the metabolic rate is slow to rise to this increased level and therefore an increase in venous-blood concentration will occur. This results in a change in the signal that is detected. Aside from the image alternation it will cause, it can also be used to measure blood flow and perfusion. The BOLD contrast can locally see where the blood vessels are using oxygen due to relative changes in oxygenation levels.

2.2.5 FAIR Technique

There are some newer techniques that are used to measure perfusion imaging in MR. One is the advanced methods of quantifying an arterial spin tagged method is called Flow-Sensitive Alternating Inversion Recovery or FAIR. [6] [7] This method uses two images as a comparison, the first with a slice selection inversion pulse, and the second without a slice selection inversion pulse as a control. This method takes continuous images of both the control and stimulated periods. The blood flow changes can be directly determined from the relative signal changes in FAIR. This technique does not use any contrast agent, which makes it very advantageous.

Another advantage of FAIR is its ability to quantify the perfusion. [7] The way to obtain a quantified blow flow through the FAIR technique is by collecting measurements of the magnetization, Mo, and T1. This has been done with some success, but it is not yet as

accurate in quantification as SPECT or PET. With the evolving importance of noninvasive perfusion measurements, the future for FAIR quantification is promising.

The most common application of MR perfusion is of cerebral blood flow. [2] [3] The measurement of brain perfusion for stroke victims especially, is very important. Often much of the brain tissue is damaged or dies after a stroke. For many years the only way to quantify and image brain perfusion was SPECT and PET. Yet the spatial resolution of these methods and others are low in comparison to MR imaging. The higher resolution and the usage of non-ionizing radiation make MR perfusion imaging a vast improvement. As the MR techniques improve, the developed MR perfusion imaging is expected to be the most widely used and accurate 3-D perfusion imaging method. Advances in MR assure the future for MR perfusion imaging.

2.3 Continuous Perfusion Measuring

While these MR methods offer a perfusion measurement, they do not offer continuous monitoring. Continuous quantification of the cerebral perfusion allows better management of patients with compromised perfusion, and the best chance for tissue survival and retained/restored function. One method to measure blood perfusion continuously in real-time is using the thermal diffusion probe (TDP). The fundamental theory behind the TDP is that flowing blood carries heat away from the heat source convectively at a rate proportional to the flow.

The probe consists of a long polyurethane catheter that is 1mm in diameter. Two mixed

metal oxide thermistors serve as the sensors: an active one at the distal end and a smaller

passive one that is a few millimeters proximally. A thermistor is an electrical resistor,

whose resistance has strong temperature dependence. The active thermistor is heated 2°C

above initial tissue baseline temperature. The passive thermistor continually measures

the baseline temperature and continually updates the ΔT between the heated tip sensor an

the tissue baseline. The measurement field is approximately a 4mm diameter sphere with

the active bead at the center. Perfusion is extracted by the power-time data required to

maintain the active sensor at a certain temperature.
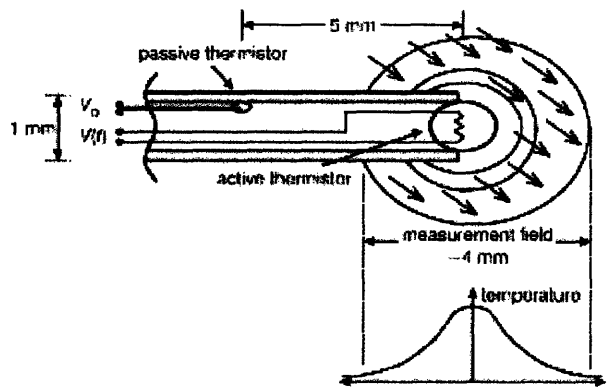
Figure 2.1 Schematic of the thermistor tip. Reproduced from Martin et al. [1].

Within in biological tissue, thermal energy in the form of heat is dispersed by conduction

through the tissue and by convection with the flowing blood. The additional heat from

the active thermistor, is thus also dissipated by conduction and convection. The

convection term is the one of interest, as it permits the quantification of blood perfusion.

In order to accurately quantify blood perfusion, the conduction component must be

subtracted from the total heat transfer. Tissue conductivity can be simultaneously determined from the power-time data before the convective affect is developed. The perfusion extraction algorithm is complex. The model is derived from the governing equations of heat transfer in biological tissue. The coupled biological heat transfer equations of the tissue and the embedded TDP are as follows:

$$\frac{1}{\alpha_m} \frac{\partial T_m}{\partial t} = \nabla^2 T_m - \frac{\omega \rho_{bl} c_{bl}}{k_m} T_m \qquad (2.1)$$

$$\frac{1}{\alpha_s} \frac{\partial T_s}{\partial t} = \nabla^2 T_s - \frac{1}{k_s} \frac{P}{V} \qquad (2.2)$$

Where:

T_m = temperature elevation of the tissue

α_m = thermal diffusivity of the tissue

k_m = thermal conductivity of the tissue

ω = local diffusion rate

ρ_{bl} = density of the blood

c_{bl} = specific heat of the blood

T_s = temperature elevation in heat bead

α_s = thermal diffusivity of heat bead

k_s = thermal conductivity of heat bead

P = power dissipation

V = volume of heat bead

To use these equations for the probe-tissue system, there are certain assumptions that are used. It has to be assumed that the system acts in an ideal way, assuming that the heated bead is spherical, the thermal contact is perfect and the volume of the heated tissue is at least 5-times larger than the probe dimensions. Its also assumes that bio heat transfer laws govern. Solutions of the coupled probe-tissue thermal equations with appropriate initial and boundary conditions give rise to the time dependent temperature fields in both the tissue and probe which can be used to isolate the local perfusion in terms of power, applied temperatures, and intrinsic thermal properties.

$$\frac{P}{4\pi a k_m \Delta T} = \frac{1}{\dfrac{k_m}{5k_s} + \dfrac{1}{1+\lambda a}}\left[1 + \frac{\dfrac{a}{\sqrt{\pi \alpha_m}}f(t)}{\dfrac{k_m}{5k_s}+1+\lambda a}\right]$$

where

$$f(t) = \frac{e^{-\lambda^2 \alpha_m t}}{\sqrt{t}} - \sqrt{\pi \lambda^2 \alpha_m}\, erfc\left(\lambda a \sqrt{\frac{\alpha_m t}{a^2}}\right) \qquad (2.3)$$

$$\lambda = \sqrt{\frac{\omega \rho_{bl} c_{bl}}{k_m}}$$

Where:

$\Delta T = temperature\ gradient$
$a\ = thermistor\ radius$

In the TDP system, an onboard computer processes the acquired data in real-time through highly developed algorithms to obtain perfusion measurements as a function of time. This system has been validated through clinical experiments. It has shown to be in agreement with other proposed methods such as hydrogen clearance, Xenon-CT, and radioactive micro spheres. [1] [9] The TDP is being used in clinical setting. There is great interested to have the TDP perfusion probe work within a magnetic resonance (MR) environment. As more devices are used intraoperatively, a device that continuously monitors blood flow would be of high clinical value. Before the TDP can be placed inside the MR environment, there has to be a thorough assessment of the implications. This thesis looks at the some of these considerations.

Chapter 3 - NMR Basics

3.1 NMR Theory

One of the projects applications is Magnetic Resonance Imaging (MRI). In order to make design and other considerations, it will be useful to provide Nuclear Magnetic Resonance (NMR) and MRI basics.

Every type of nuclei reacts to a magnetic field in a certain unique way. If a magnetic field is induced, it will affect the spin and orientation of a nucleus. Measuring this affect is the basis of NMR imaging. [5]

Nuclei with an odd number of protons or neutrons, i.e. nonzero nuclear spin, have angular momentum. The nucleus of interest is 1H or the proton. The human body mainly consists of water and fat, making the proton the most useful nucleus to study. Considering the nucleus has a charge and it is spinning due to its angular momentum, a magnetic field is created is created. This is called the nuclear magnetic moment and denoted by μ. The total angular momentum, $\mathbf{J}$, is related to the magnetic moment through the gyromagnetic ratio, γ. Each type of nuclei has a specific γ.

$$\mu = \gamma \mathbf{J} \quad \text{where} \quad \mu = \gamma \hbar \mathbf{I} \qquad (3.1)$$

The angular momentum is related to the dimensionless angular momentum operator or spin, **I**, through Plank's constant, $\hbar$. The eigenvalues for the z-component of the angular momentum, **I**, is $m = I, I-1,\ldots, -I$. Protons have a spin quantum number of $I = 1/2$. If a nucleus is put into a static magnetic field, **Bo**, that is defined along the z-axis, the interaction energy (defined as $E=\mu\cdot\mathbf{B}$) becomes:

$$E = \gamma m \hbar \mathbf{Bo} \qquad (3.2)$$

For a proton where $I=1/2$ making $m = \pm\frac{1}{2}$, the energy levels available to the spins are $E=\pm\frac{1}{2}\gamma\hbar\mathbf{Bo}$. The allowed transitions are $\Delta m = \pm 1$, making the energy level difference:

$$\Delta E = \gamma\hbar\mathbf{Bo} \qquad (3.3)$$

This corresponds to the energy level difference being related to the applied static field and the gyromagnetic ratio. The gyromagnetic ratio for a proton is 42.6 MHz/Tesla.

From equation (3.3), the resonance frequency can be determined. Considering that, $\Delta E = \hbar\omega$, this give the relation called the Larmor Frequency, ω_L:

$$\omega_L = \gamma\mathbf{Bo} \qquad (3.4)$$

This is the precise frequency of allowed energy transitions. If a certain nucleus is being studied, this frequency is applied and the spin states can make their transitions.

Without an applied magnetic field, there is no preferred orientation of the protons. Overall they produce no net magnetization. When a strong magnetic field is applied, the magnetic moments of the protons align parallel or antiparallel to the direction of the field. Although they align with and against the field, there is an overall bias toward the direction of the magnetic field because it has a lower energy state. Thus, there is a resultant macroscopic magnetization in the line of the applied field. When the field is applied, there is a change in the angular momentum ($dJ/dt = \mu \times \mathbf{B}$) which equals the torque. From this equation we can derive the net magnetization, $\mathbf{M}$, where $\mathbf{M} = \sum \mu$.

$$dM/dt = \gamma \mathbf{M} \times \mathbf{B} \tag{3.5}$$

The resultant cross product corresponds to a rotation of the magnetization around the magnetic field. Thus, the net magnetization, $\mathbf{M}$, precesses around the applied magnetic field, $\mathbf{B}$, at the Larmor Frequency, $\omega_L = \gamma \mathbf{B}$. Considering there are other forces and interactions on the molecules, the magnetization does not precess forever in the direction of the applied field. Instead it reaches its net magnetization that is dependant on the thermal equilibrium value of the magnetization, Mo.

$$Mo = \gamma^2 \hbar^2 Bo/4kT \tag{3.6}$$

The thermal equilibrium magnetization has a dependency on the Boltzmann energy, kT. To make the spins of interest more manageable conceptually and in the equations, the

frame of reference is changed. In the laboratory frame, the frame is stationary and the spins are precessing. In the rotating frame, the frame is precessing at the same rate making the spins look stationary. Each arrow represents a spin precessing about the static field. When their z-plane component is summed, they have a net magnetization about the z-axis.
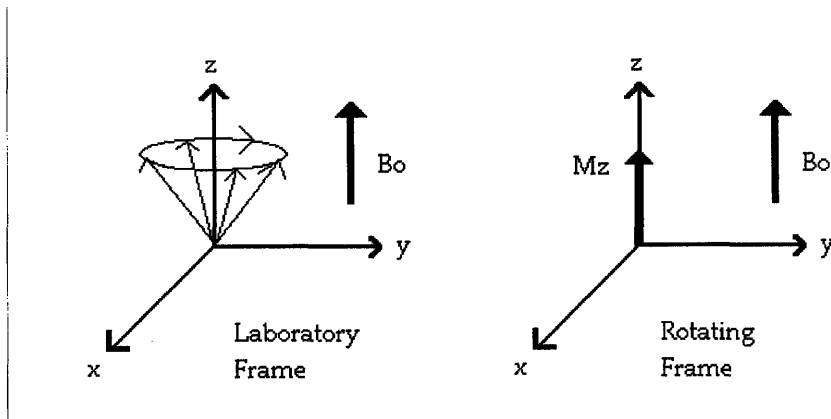
Fig. 3.1: Diagram of the Laboratory and Rotating Frame of reference.

If another magnetic field, B_1, is applied in the perpendicular direction to the static field, the net magnetization, Mo, will be disturbed from its equilibrium position. The magnetization will not stay in this new direction; instead it will relax back to the equilibrium value. This is precisely what is done in NMR. A radiofrequency pulse is applied perpendicular to the static field, causing the protons to instantaneously align with the pulse. The system relaxes through two methods: longitudinal and transverse relaxation, with time constants T1 and T2, respectively.

Longitudinal relaxation, also known as spin-lattice relaxation, brings the z-component of the magnetization back to its maximum value in the direction of the static field. Spin-lattice relaxation is dependent on the spins losing energy to its surroundings or lattice, and it is denoted by T1. After the rf pulse, the magnetization in the z-direction goes to zero. Over time, the protons realign to their maximum vertical position.

$$M_z(t) = M_0 \left(1 - e^{\frac{-t}{T_1}} \right) \qquad (3.7)$$

Transverse relaxation, also known as spin-spin relaxation, relaxes the magnetization in the x-y plane. It is dependent on the intrinsic properties of the sample and the field. The magnetic field is not exactly equivalent at every proton, causing each one to have a slightly different precession. After a while it will cause a fanning out effect of the net magnetization in the rotating frame, hereby decreasing the magnetization in the x-y plane. The localized magnetic fields inside a magnet are not completely homogenous, thus there is transverse loss due to these inhomogeneities. This is denoted through T2*, and is measured experimentally. T2* is always less than T2, meaning that experimentally the transverse magnetization decays faster than the theoretical value.

$$M_{x,y}(t) = M_0 e^{\frac{-t}{T_2^*}} \qquad (3.8)$$

Putting it all together, equation (3.5) needs to be modified to incorporate the relaxation from the system. This is known as the Bloch Equation.

$$\frac{dM}{dt} = \gamma(M \times B) + \begin{bmatrix} Mx/T2 \\ My/T2 \\ (Mo - Mz)/T1 \end{bmatrix} \qquad (3.9)$$

Inside the system, there is also magnetization loss from the diffusion of the moving spins. The magnetization equation can now be described by the Bloch-Torrey equation which takes into account the relaxation and diffusion of the system. Where **D** is the diffusion coefficient and **v** is the flow.

$$\frac{dM}{dt} = \gamma(M \times B)$$

$$+ \frac{(Mo - Mz)\hat{k}}{T1} \quad T1 \ relaxation$$

$$- \frac{(Mx\hat{i} + My\hat{j})}{T2} \quad T2 \ relaxation$$

$$- \nabla \bullet \mathbf{v}M + \nabla \bullet \mathbf{D} \bullet \nabla M \quad diffusion$$

$$(3.10)$$

This equation provides the basis for NMR imaging.

The relaxation of the protons in the x-y plane produces a frequency that can be picked up by the NMR machine. An oscilloscope detects the signal that is generated by the resultant small currents from the dephasing of the magnetization. The signal generated displaces a decaying cosine wave, as described by equation (3.8). The resultant wave is

called the free induction decay (FID). The information within the FID is a time domain signal. Using a Fourier transform, the data can be turned into a signal function that is dependent on frequency. The signal is also dependent on the number of protons dephasing. By manipulating the new orthogonal magnetic field, B_1, a signal can be detected from the sample. The field is created by inducing a magnetic field inside a coil that is surrounding the patient.

An important aspect of NMR imaging is the addition of a gradient field. In order to resolve the distribution of spins in space, a spatially varying magnetic field is added to the system. The main premise behind the gradient is to provide an environment where each region of spins experiences a unique magnetic field, and thus precess at different rates. If the electrons are precessing at spatially dependent magnetic fields, then that corresponding frequency can be specifically collected in the readout. This allows for a two-dimensional image to be taken from a three-dimensional object.

A specific gradient is purposely added to the system to resolve a spatially dependent area. There are many types of gradients that can be implemented in any combination of the x, y, and z-planes; they are denoted by G_x, G_y and G_z. Often certain gradients are used in pulse sequences as certain combinations can elicit specific results. For the purpose of the thermistor application, it should be understood that there are three fields in an NMR environment. Depending on the sequence, the strength of the static field is going to depend on the gradient used. Even if the thermistor probe is not in the selected slice, it is going to feel the affects of all three magnetic fields.

This presents the basics for NMR Imaging. The details past this point go beyond the scope of this thesis. The aspect of interest here is the magnetization of the tissue and how it will be affected by the three external magnetic fields.

3.2 Phase Encoding to Study Velocity

Images are density dependent, meaning that the data retrieved depends on the number of protons within the sample slice. The most accurate images are constructed when the sample is entirely stationary. Yet, in reality, a person's body is continually moving; as the heart continues to pump blood throughout the body, and the lungs continue to breathe. Considering nuclear magnetic resonance provides a two-dimensional slice of a three-dimensional sample, this property can be utilized to help determine internal movement, like blood flow or pulsatile movement.

When the NMR pulse selectively excites a specific plane of interest, only those protons are going to get phased. Within that plane, the protons have the same frequency. If there is motion, then some or all of the moving particles will exit the plane; resulting in less detected spins for regions of movement. For example, if a slice of the brain is being imaged that has an artery, all the protons within that slice will be affected by the rf-pulse. As they are dephasing, the protons in the blood will leave the selected slice and thus not contribute to the detected signal. The static tissue will have a higher resultant frequency

than the moving blood. The velocity of the flowing material, will determine the strength of the signal void. If the velocity is fast enough, there could even be no signal detected.

To quantify velocity using this technique, the flowing area is compared to the static surrounding areas. This is done by a comparison of the data retrieved on each pixel follow a pulse sequence. Specific sequences are constructed that will allow for an accurate measurement of signal changes due to velocity. The method used most often is called the Phase Contrast Sequence, or is some modification of this sequence. It has been verified through many experiments. [10] [11] After velocities are found on a pixel basis, it is multiplied by the pixel area to obtain the flow volume. This quantity is typically measured in millimeters/sec, ml/sec.

Another application of this technique is to measure internal tissue movement. The same theory applies. If a tissue is moving, the moving area within the selected slice will exit the reading area and have less apparent spins on the reconstructed image. In the subsequent chapter, many of the studies that provided results for brain motion were done with this type of imaging technique.

3.3 Interventional MRI

Magnetic resonance imaging (MRI) is a widely used practice that offers many benefits in comparison to other medical imaging techniques. To date, MRI has the best soft tissue contrast of all medical imaging. It has the ability to show biological tissue pathology to a

very precise degree, and tissue can be observed on many different planes without resituating the patient. The images are taken very rapidly, and the patient is not exposed to ionizing radiation. MRI also has the capability to measure additional physical and functional variables including blood flow, and temperature, offering more information to the operator. The added information and precise images, makes MRI especially important in the field of interventional work.

There are two types of interventional MRI techniques. The first is conducted initially at the magnet site, where an abnormality is located and instruments positioned around it. The patient is then removed and the procedure is done outside the magnet field. This technique has the advantage of using higher field strengths for imaging, as well as non-compatible instruments for the specific procedure.

The more widely used interventional MRI technique takes images and conducts the procedure within the imaging volume. The MR images are used in real-time as a guidance and monitoring system. Within this open MR scanner, more complex procedures can be completed, but access to the patient and corresponding instruments is a factor. For this system, there are three different methods that utilize a low-field, medium-field, and a high-field. The low field does not offer a high enough resolution for most interventional procedures. High-field is the commonly used 1.5 T magnet, which often does not permit the required amount of space for an operator to perform on the patient. The mid-field is the best combination of both; it offers ample room and images that are of high enough resolution to be used as a guidance system.

The benefit to interventional MRI is the ongoing images of the patient while a procedure

is being preformed. The magnet is usually set up in a doughnut shape with the patient in

the middle. A surgeon has a better diagnostic and monitoring system to warrant a more

favorable outcome, especially with surgeries where the abnormalities can only be seen on

an MRI. The surgeon can see inside the patient's body without physically entering.

Gaining more information about the patient is extremely important, along the same lines,

more information for the surgeon is also beneficial. Having a device that continuously

measures blood perfusion would be extremely helpful and important for an interventional

application. Yet, before it can be used intraoperatively, the affects of the magnetic field

on the TDP have to be determined and more fully understood.

Chapter 4 - Movement of the Brain, Spinal Cord, and Cerebrospinal Fluid

4.1 Introduction to Brain Motion

In monitoring brain perfusion, numerous situations were found in which the data from which perfusion is extracted revealed behavioral characteristics which could best be explained if periodic brain tissue motion existed. Periodic tissue relative motion could only exist if there were motion of the brain within the skull. As I was already investigating what it would take to render the TDP MR compatible with the intent in using it in an MR field; and since MR is increasing being used to provide near real-time 3D quantitative maps of brain perfusion and since physiologically induced brain motion is a concern for MR images distortions – I decided to investigate the possibility of whether the brain motions recoded in the MR literature had any bearing on the motion like artifact observed in the TDP perfusion data. Consequently, this effect has added as a second focus of my thesis. Hopefully a study of the motion of the brain will offer an explanation and present a possible route to modify the perfusion algorithm, making brain perfusion measurements more accurate in the presence of such motion or offering a way to avoid this issue.

It was noticed that the artifact was producing a sinusoidal rhythm that was not in phase with the heart beat or the respiration rate. At first it was thought to be directly related to the blood flow through the brain, but later determined that there are many different

causes of brain motion, namely blood flow, cerebral spinal fluid, and respiration. Each of these is independent and dependent upon one another. The complexities of the human body, especially with the head, go beyond the scope of this thesis. I will offer a valuable overview of the system and a big-picture suggestion of how to fix the problem.

4.2 Functional Anatomy

4.2.1 Cardiac System

I will first comment on the cardiovascular system. The cardiovascular system plays an integral role in the movement of the brain. The blood that enters and expands the brain is dependent upon the periodic contractions of the muscles in the heart. To understand how and when the brain is expanding, first the cardiac system must be assessed. [14][15]

The heart and its blood vessels can be split into two sides that serve different functions, the left and right. Each side has two chambers, the atrium, which is positioned above the second and larger chamber, the ventricle. The right side pumps blood through the pulmonary circulation, which brings deoxygenated blood to the lungs to become oxygenated. The left side of the heart pumps blood to the rest of the organs in the body, exiting the ventricle through the aorta. The cardiac system follows this main progression. Oxygenated blood fills the left ventricle from the left atrium. The heart contracts, ejecting the blood through the aorta to be distributed to the rest of the body's organs. The blood is collected in the vena cava and on its way back to the heart. It enters the right

atrium, and fills into the right ventricle. Upon contraction again, the deoxygenated blood exits through the pulmonary artery to the lungs. From the lungs it travels through the pulmonary vein back into the left atrium to begin the process again.

Heart contraction has to do with specialized myocardial cells that have high electrical excitability. When prompted, the cells carry an action potential that causes a depolarization of the cells following a repolarization back to the resting membrane potential. Due to the concentration of ions on the inside an outside of the cell membrane, each cell has a certain conductance potential, which is measured in millivolts. The action potential causes ion channels to open quickly making the membrane potential less negative, this is called depolarization. As the action potential propagates to the next cell, the ion channels close and the cell slowly resumes its original membrane potential, thus repolarizing. After a certain refractory period, the cell is ready for the next action potential. The depolarization and propagation of an action potential is what occurs in the heart causing its characteristic features.

The following electrocardiogram measures the electrical activity of the heart. This is a typical diagram for a healthy heart. Each of the areas marked by letters represents important stages in the cardiac cycle. The heart is depolarized, and repolarized as the action potential propagates, and this becomes important in the chronological assessment of the occurrences.
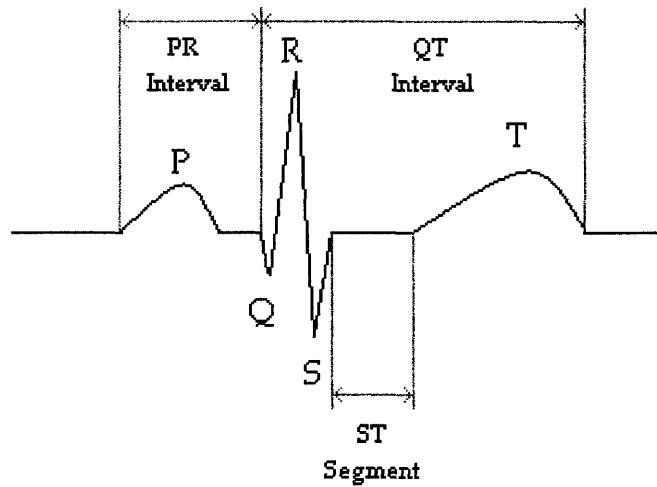
Fig 4.1: Electrocardiogram of a typical heart wave.

The potential is negative at the bottom going to positive at the top.

1. The P-wave corresponds to the depolarization and contraction of the atria forcing blood to fill the ventricle. The electrical impulse starts in the right atria and depolarizes both atriums. The depolarization of the heart travels down the muscle walls from the top of the atria to the bottom of the ventricles.

2. The P-R Interval is the time from depolarization of the atria to the start of depolarization of the ventricles.

3. The Q-R-S interval is three different waves that collectively represent the depolarization of the ventricles, and the contraction of the ventricles. The ventricles contract until the pressure inside the left ventricle exceeds the left atria, closing the mitral valve. This occurs approximately at the peak of the R-

wave. The ventricle continues to contract until it exceeds the pressure in the aorta, and the aortic valve opens expelling highly pressurized blood into the arteries. This occurs a few hundred milliseconds past the Q-R-S interval.

4. The R-wave is the most prominent of all the waves. The heart rate is typically recorded from R-wave peak to the next R-wave peak.

5. The S-T segment represents the end of ventricular depolarization to the beginning of repolarization.

6. The T-wave corresponds to the repolarizaton of the ventricles.

7. The Q-T Interval is the time from the beginning of ventricle depolarization to the end of ventricle repolarization.

The shape of the electrocardiogram will help to understand the motion in the brain. In the subsequent section, brain motion will be analyzed. Many of the reports use the R-wave as a marking point for their analysis.

4.2.2 The Brain

The brain contains a high percentage of the body's oxygenated blood. It has the highest density of capillaries, with the gray matter being denser than the white matter. This corresponds to the neurons needing more blood to perform actions. The brain has no way to store energy, and thus it needs a constant supply of oxygenated blood. Any compromise to this delicate system can cause neural damage within seconds of ischemia. [16] To fully understand how the blood is flowing, anatomical direction need to be established. The orientation of the corresponding structures within the human brain has the following conventions.

Anatomical Planes
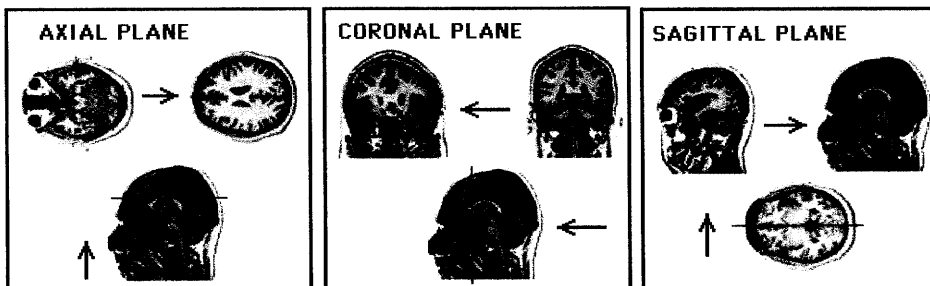
Anatomical Orientations
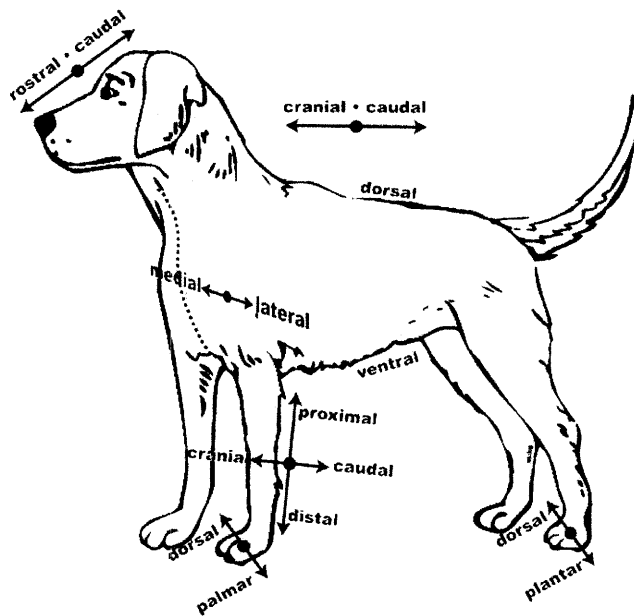
Terminology:

Inferior – Lower

Superior – Upper

Anterior or Ventral – Toward front

Posterior or Dorsal – Toward back

Cephalad or Cranial – Toward Head

Caudal or Caudad – Toward Tail end

Medial – Toward midline

Lateral – Away from midline

4.3 Blood Flow

Recently oxygenated blood travels from the left ventricle through the aorta, which is the main artery in the body. The aorta forms an arch, where two subclavian arteries branch off carrying blood straight to the brain. The two subclavian arteries, common carotid and vertebral, branch to form the two pairs of arteries that feed the brain: the internal carotid arteries, and the vertebral arteries. The internal carotid arteries supply most of the cerebral hemisphere, while the vertebral arteries mainly supply the brainstem, cerebellum, and spinal cord. The internal carotid arteries ascend bilaterally through the neck into the base of the brain at the circle of Willis. The vertebral arteries come together at the base of the brain and form the basilar artery which then feeds into the circle of Willis. Due to the delicate pressure gradient of each artery, there is not much motion around the circle of Willis. If an artery is compromised, the circle of Willis can act as a mechanism to supply more blood.
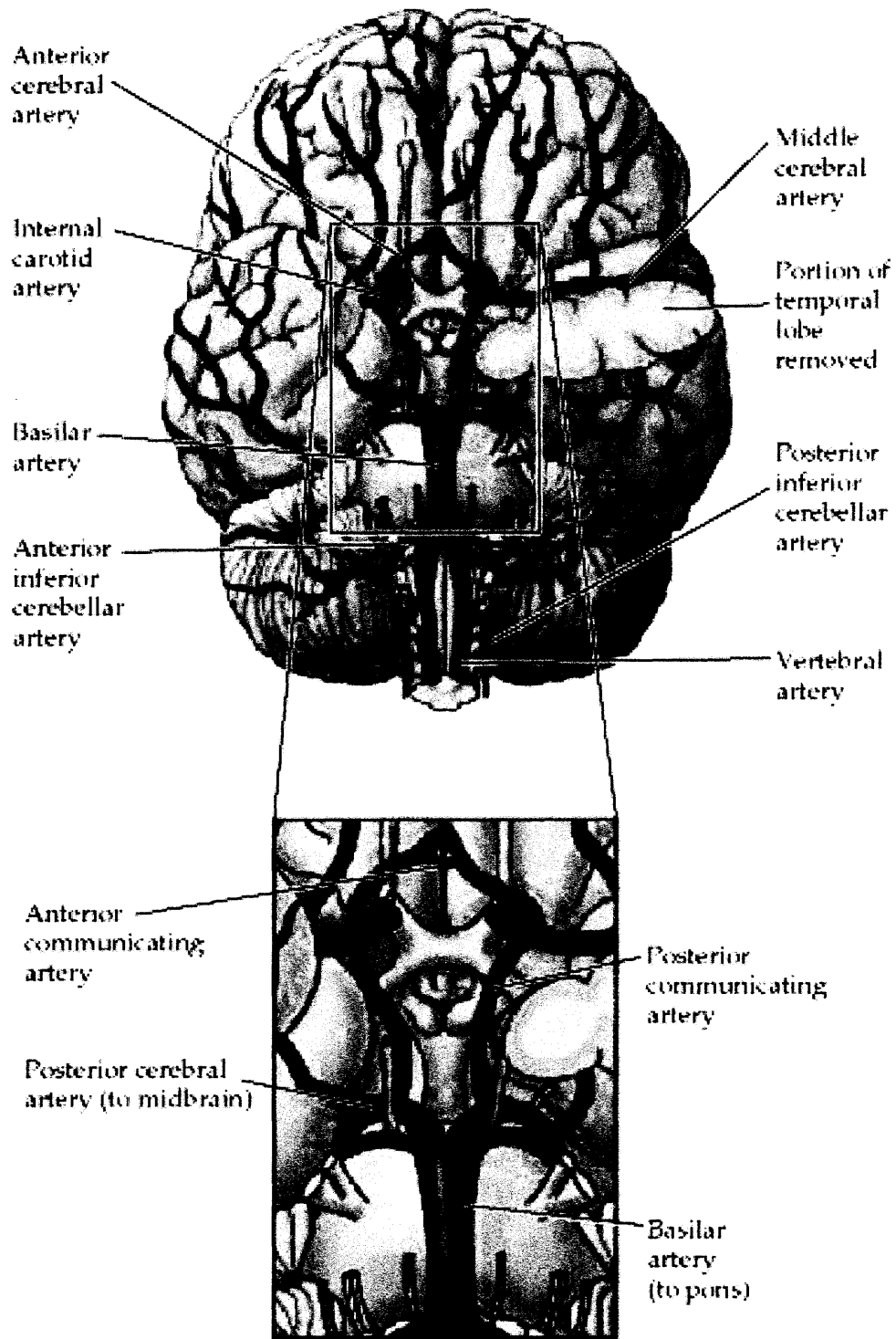
Fig 4.2: The arterial blood supply to the brain from the Circle of Willis. Reproduced

from Purves et al. [14].

The internal carotid arteries branch forming two important cerebral arteries; the anterior cerebral artery and the middle cerebral artery. Both of these supply the forebrain with blood. The anterior cerebral artery travels from the circle of Willis in an anterior, then ascending direction, circumventing the lateral ventricle. The middle cerebral artery feeds the outer part of the forebrain. These arteries branch further to supply the cortex and the basal surface of the brain, as well as deeper structures including the basal ganglia and the thalamus.

The posterior area of the brain is supplied by three main arteries, the vertebral, basilar and posterior cerebral basilar. Before the vertebral arteries join to become the basilar arteries, they continue to branch creating the blood supply to the posterior part of the brain. The posterior circulation supplies the midbrain, brainstem, and posterior cortex.

(B)

Anterior
cerebral artery

Posterior
cerebral artery

Middle
cerebral artery

(C)

Posterior
cerebral
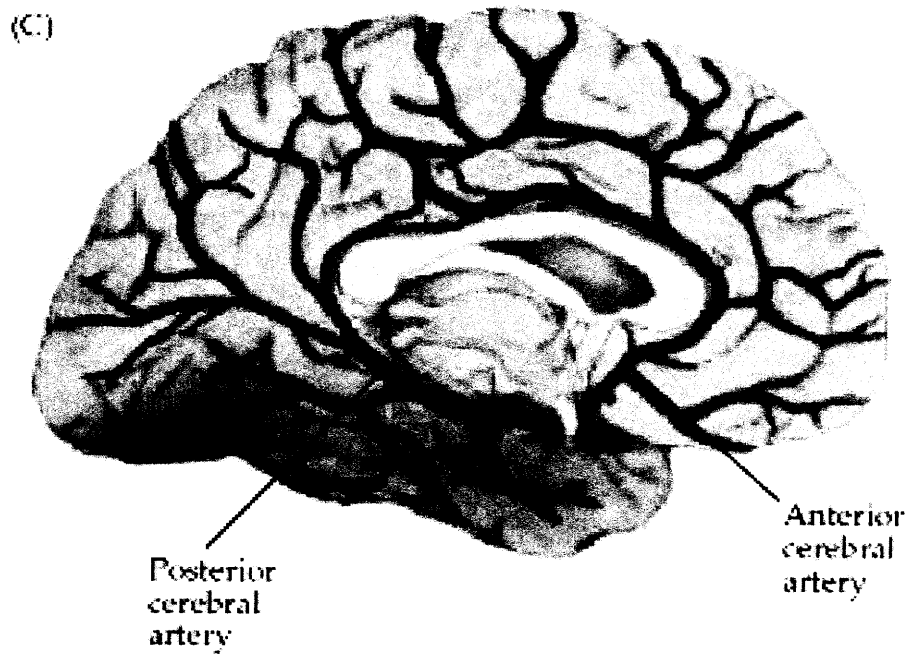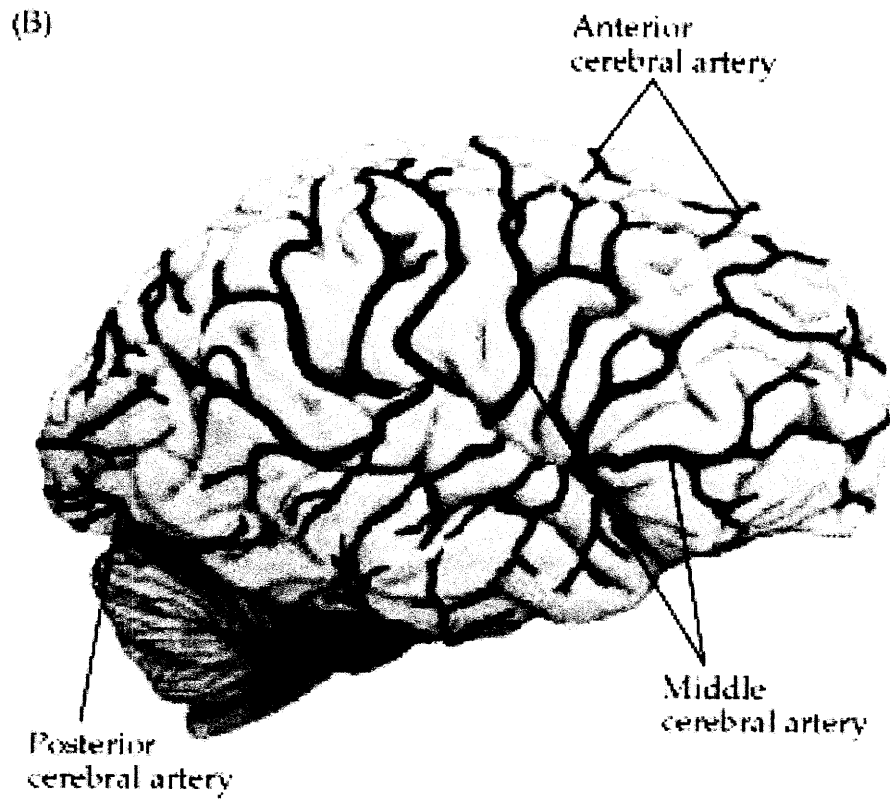artery

Anterior
cerebral
artery

Fig 4.3: The location of the main arteries in the Brain. Reproduced from Purves et al [14].

The blood leaves the branches of the arteries and enters the capillary bed. This causes the largest swelling of the brain. After the oxygen is taken up by the brain cells, the deoxygenated blood enters the venous system. The venous system is less complex than the arterial system. The blood velocity is significantly slower, and the veins are primarily receptacles for the deoxygenated blood. The main vein of the brain runs down the middle of the brain between the two hemispheres. It is called the superior sagittal sinus, and it runs from right behind the forehead to the very back of the neck. At the base of the neck, it bifurcates and transcends down the neck through the internal jugular vein. The deep arteries of the brain empty into the straight sinus, which also joins at the back of the neck. Veins have much thinner walls than arteries. They have no muscular components and blood is moved through them from the pulsatile motion of arterial blood.

4.4 Cerebral Spinal Fluid

Many studies have shown that there is movement of the brain and spinal cord inside the body. Studies have also shown that the cerebrospinal fluid, which incases both of these structures, also has a flow. It has been noted by many that the brain and spine move in a piston-like fashion. [17][18][19][20][21]

The circulation of the cerebrospinal fluid is a complex and not completely understood phenomenon. The ventricular system of an adult brain has a volume of about 120-160ml of cerebrospinal fluid and on average produces at about 500ml/day. The density of the liquid drastically decreases the weight of the brain. [16][33]

Cerebral aqueduct

Fourth ventricle
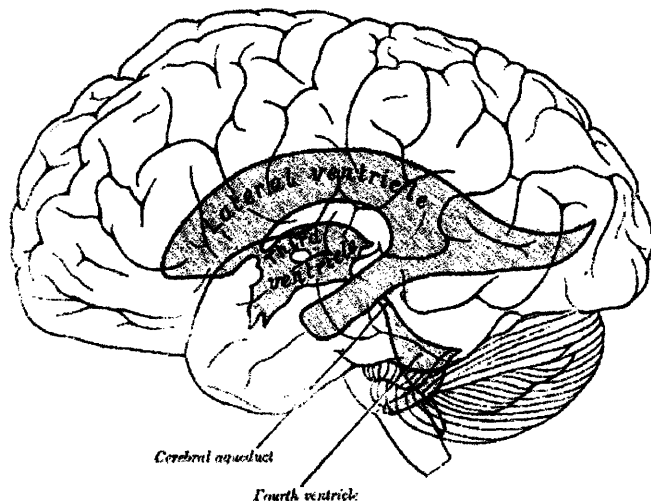
Fig. 4.4: The ventricles oriented inside the brain. Reproduced from Gray's Anatomy [24].

CSF is created by the choroids plexus which are thin capillary cells that line the ventricles. The CSF travels from the choroids plexus into the lateral, third and fourth ventricles. It flows around the subarachnoid space surrounding the brain, and also travels down the spinal canal. Within the spine, there is circulation about the spinal cord and central canal. [33] Fluid motion in the spine is helped by physical movement of the vertebrae, as well as the pulsatile motion from the brain and spinal cord.
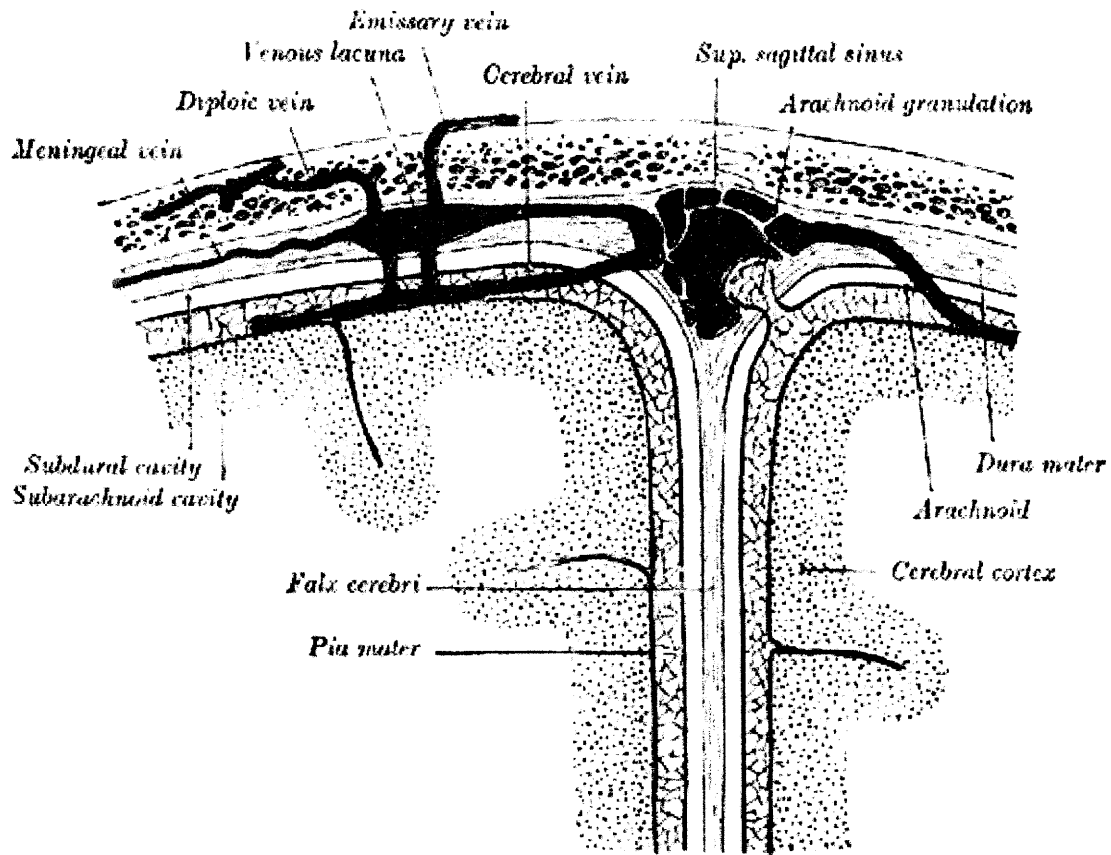
Fig. 4.5: Coronal view of the upper part of the brain and skull. Reproduced by Gray's Anatomy [24].

The absorption of the CSF was originally thought to be in the arachnoid granulations, which are projections from the arachnoid layer into the venous sinus. Recently, it has been discovered that CSF is absorbed by the capillaries through the delicate balance of osmotic pressure within the vascular system. [21] Thus, the absorption is governed by the Starling hypothesis, which states that capillary membrane filtration is proportional to the hydrostatic pressure gradient minus the osmotic pressure gradient. To maintain homeostasis, and ultimately counter the production rate of the CSF, there is an equal amount of absorption by the capillaries of the central nerves system. [21] Considering

there is fluid flow across the cerebral capillary membrane, some of the interstitial fluid passes through the capillary membrane into the CSF, thus there is a small variation between the CSF at the brain and the CSF at the outer edges. The interstitial fluid and CSF have similar characteristics, so overall this does not amount to much change, but still worth noting.

While there have been many theories about the flow of the cerebrospinal fluid, it has been shown that overall there is a dominant pulsatile movement of the CSF. [17] [19] [21] The ventricles have their own non-cardiac pulsations, and it is also postulated that the cranium has its own pulsatile rhythm. [33] Yet, the dominant force is the brain blood vessels filling with blood, causing the brain to move and pushing the CSF around the ventricles. Pulsatile blood flow causes non-uniform velocities of the CSF, and also causes a diffuse, multidirectional mixing of the fluid.

According to the Monro-Kellie doctrine, the volume of the brain, CSF, and intracranial blood is constant. [22] This is under the assumption that liquid is incompressible, and that the cranium is rigid. If one of the constituents increases in volume, another one has to decrease. This model is helpful in interpreting the movement of the brain and associated CSF. During systole, blood rushes into the arteries inside the brain, the brain volume expands exerting a force on the surrounding CSF. The CSF exerts an equal and opposite force against the rigid dura mater everywhere except at the opening in the foramen magnum and the tentorial notch. These are both located at the base of the brain where the spinal cord connects. The pressure from the expanding brain pushes the CSF

into this opening causing a posterior motion of the brainstem down the spinal canal. The dural layer of the spine is more elastic and can compensate for the rapid increase in volume.

There are two types of expansion following the cardiac cycle. At systole, the ejected blood volume fills the arteries, this is called arterial expansion. It accounts for expansion of the intracranial cerebral arteries and is equal to 1.5mL or the volume of systolic stroke volume at the foramen magnum and the venous sinuses. This differs from brain or capillary expansion which is a smaller expansion when the blood leaves the arteries and enters the capillary network. Brain expansion is a short time after arterial expansion, and only accounts for a .03mL volume increase. [17][21]

The arterial blood enters the capillary bed, increasing the brain size, and increasing the intracranial pressure, which puts pressure on the veins to compress and flow. [16] The cerebral spinal fluid in the cerebral subarachnoid space responds by flowing downward into the spinal subarachnoid space. The CSF leaves the cerebral space below the tentorium cerebelli, where the cerebellum and brain connect. This first response of the CSF corresponds to the peak arterial velocity. Initially the CSF flow and the arterial flow have very similar waveforms. The rapid response of the CSF to the arterial volume decreases the intracranial pressure in the subarachnoid spaces. A short time after arterial expansion, the blood enters the brain parenchyma causing a capillary expansion of the brain in all directions. This expansion puts pressure on the ventricles causing them to expel their CSF through the ventricle pathway into the subarachnoid space.
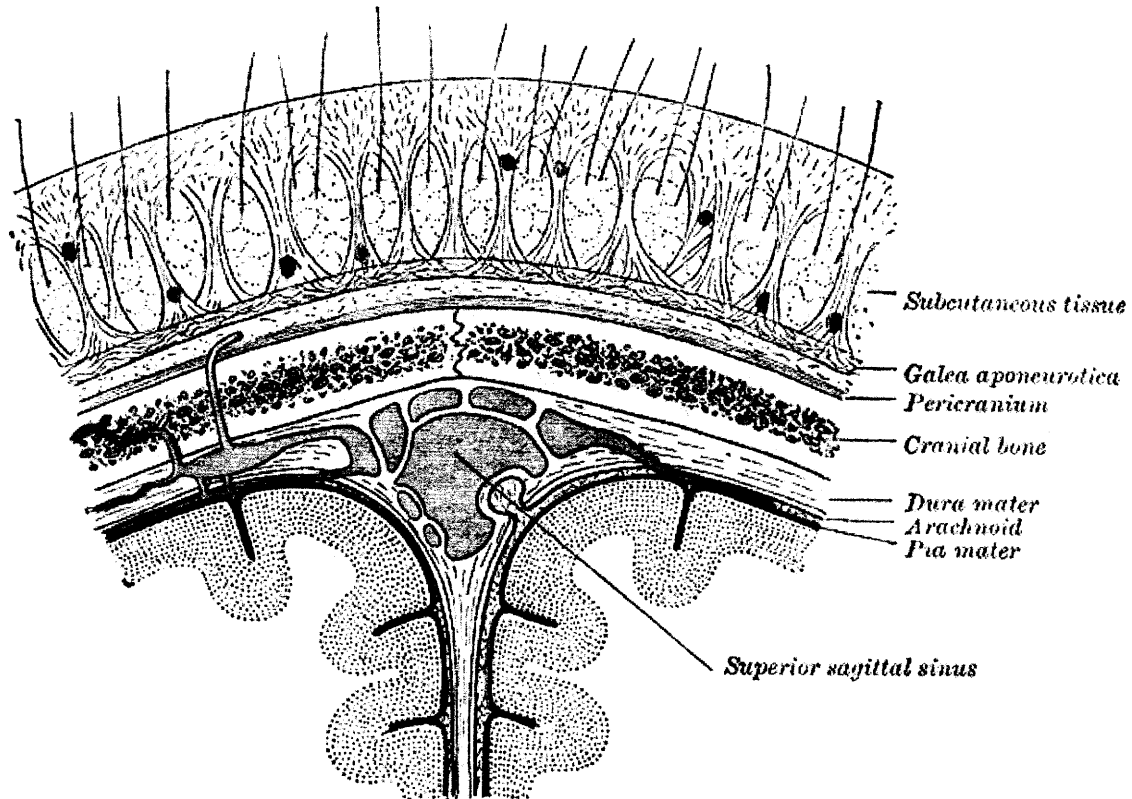
Fig 4.6: Coronal view of the scalp centered around the superior sagittal sinus.
Reproduced from Gray's Anatomy [24].

The increase in capillary expansion also increases the venous flow in the sinuses of the

dura mater, which are venous channels that drain blood into the internal jugular vein.

With the veins draining the blood out of the intracranial space the pressure decreases

causing a relatively negative intracranial pressure. In response to this pressure gradient,

the CSF in the spinal subarachnoid space flows upward to refill the cerebral subarachnoid

space. The influx of CSF pulls the brain stem away from the spine. This back and forth

motion of the CSF and the brain causes a piston-like motion of the brain, brainstem, and

spinal cord. To better understand this occurrence, Baledent et al. [23] have created a pictorial diagram.
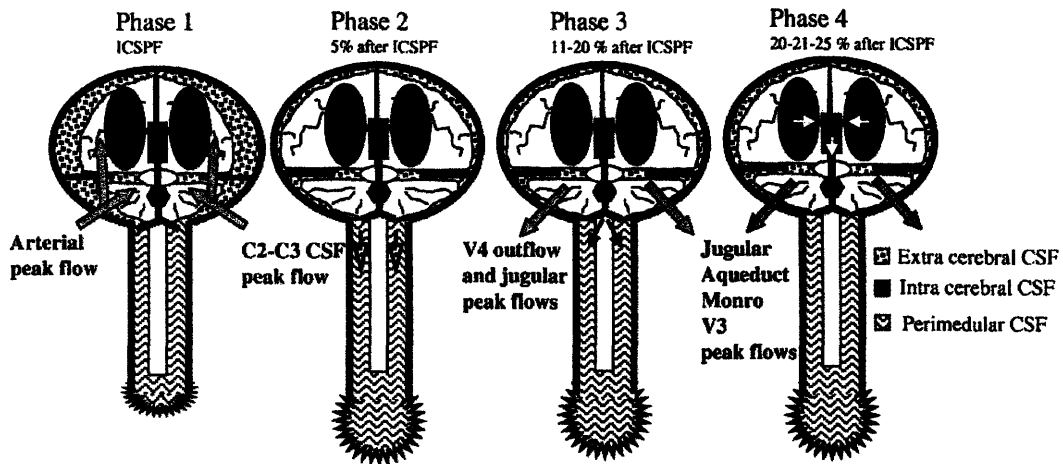
Fig 4.7: Schematic of brain and CSF to depict the movement. Reproduced from Baledent et al. [23].

The flow velocity was found from the same group to follow a near sinusoidal waveform. This study was taken between the 2nd and 3rd cervical vertebrae, which are the 2nd and 3rd vertebrae from the very top of the spinal column where it connects to the skull. The graph shows that the CSF flows initially in a caudal direction, flowing out of the head into the spinal column. After approximately half the cardiac cycle, the CSF flows back into the cranium. A pulsatile cycle is rather evident.
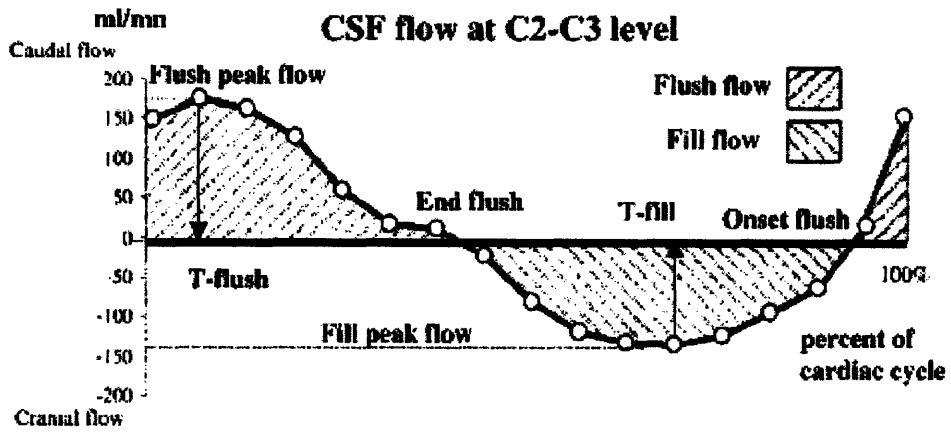
Fig 4.8: CSF flow in a caudal and cranial motion as a percent of the cardiac cycle.

Reproduced from Baledent et al. [23].

A schematic of the brain flow is as follows.
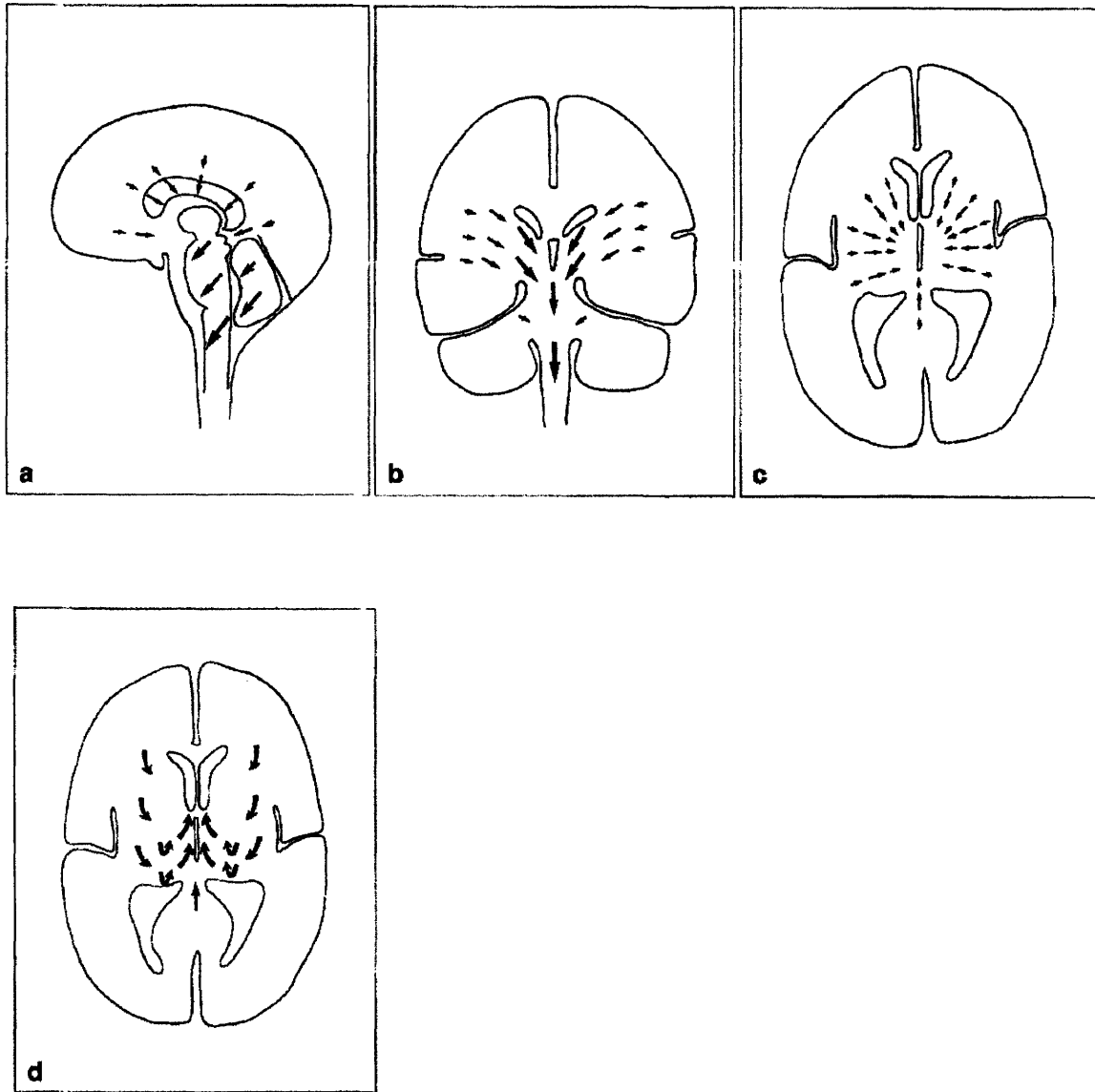
Fig. 4.9: CSF flow due to brain expansion, shown in many different planes of view.
Reproduced from Greitz et al. [17].

The brain expands, the CSF gets pushed down the spinal column, and eventually returns

up the spinal column and back into the brain. This continuous caudal-cranial motion has

been reported many times. The piston like motion of the brain and spinal cord is an

important visual for understanding the intracranial motion.

4.5 Blood Flow and Cerebral Spinal Fluid

The relation in dynamic blood flow and CSF is very well researched. Although the exact correlations are not completely understood there are many clear patterns that show there exists a definitive relation between blood flow and CSF in the head. Blood flow and CSF move in opposite directions. As blood flows into the brain and expands the capillary bed, the CSF gets pushed caudally out of the subarachnoid space into the spinal column.
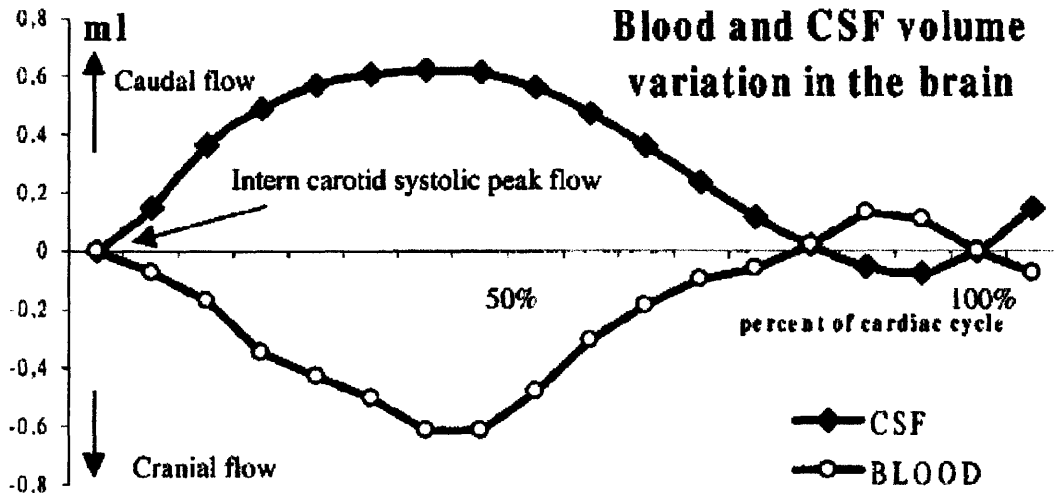
Fig. 4.10: Volume changes in the blood and CSF as a function of the cardiac cycle. Blood volume is defined as the sum of the internal carotid arteries, vertebral arteries and the jugular vein. Reproduced from Baledent et al. [23].
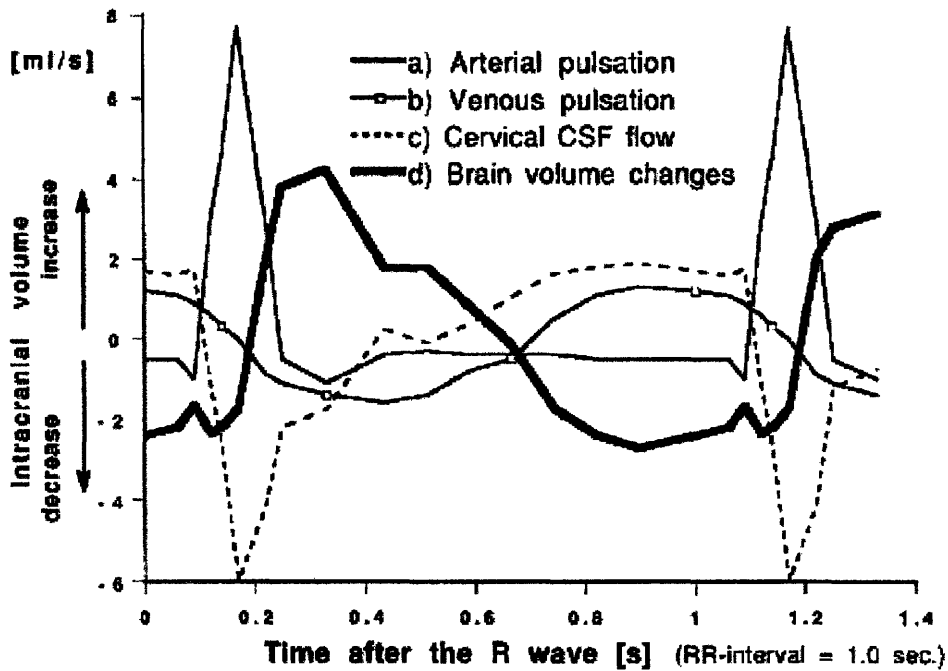
Fig. 4.11: Volume changes shown with respect to the arterial and venous pulsations. Reproduced from Enzmann et al.[18].

Many of the studies are conducted with respect to the cardiac cycle, which usually begins with the R-wave. This is an easy starting point, and a good convention amongst experiments. After the R-wave there is a certain amount of time, called the isovolumetric ventricular contraction, where the ventricle continues to contract until the aortic valve opens expelling ventricular blood into the aorta. The lag between the R-wave and the opening of the aortic valve accounts for the initial delay in volume variation. Upon aortic valve opening, the blood exists the left ventricle at a high velocity and high pressure that peaks at the T-wave or when the ventricles begin to depolarize and relax. This accounts for the continued increase in velocity after the initial ejection of blood.
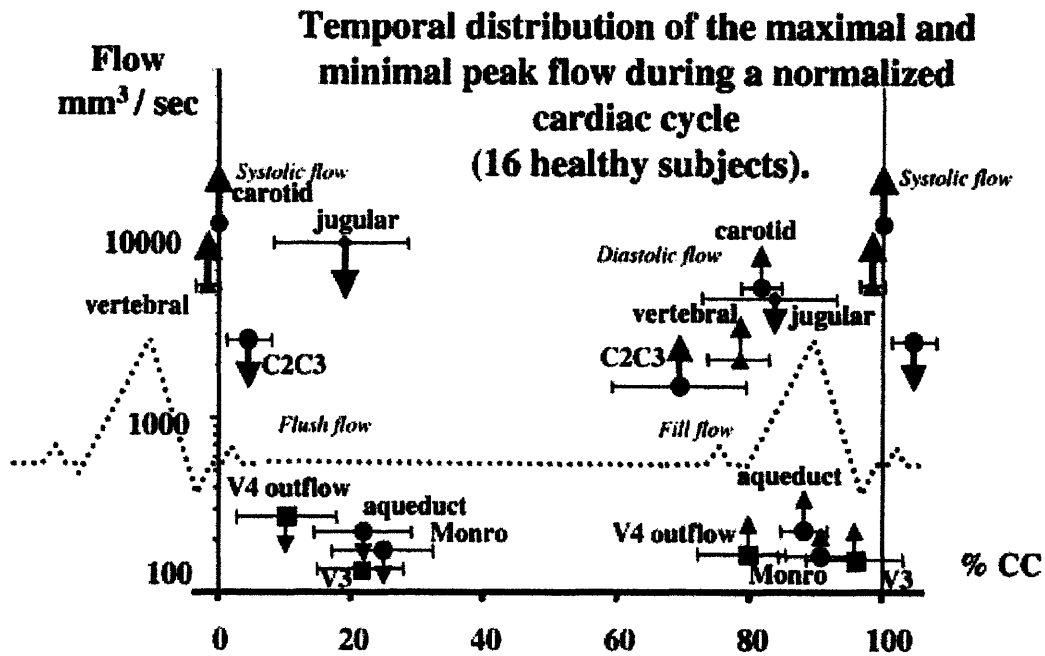
Fig 4.12: Peak flows of specific anatomical areas as a percentage of the cardiac cycle. Reproduced from Baledent et al. [23].

The schematic of Fig. 4.12 shows the relation between anatomically significant areas that are affected by peak flows. It also shows the EKG; relating the EKG waves as a function of how they affect the flows in different locations. A prominent R wave precedes the peak carotid flow, it is shortly followed by the peak flow between C2-C3, which are cervical vertebrae 2 -3 located at the very top of the spinal column.. The flow in V4, which is a lower vertebra, follows the peak flow from C2-C3; showing that the CSF flows down the spinal column. The jugular vein, aqueduct and foreman of Monro also have peak flows following the carotid flow. After a certain amount of time, the velocities reverse refilling the areas within the brain. The flowing blood and CSF causes the tissue of the brain and spinal cord to move resulting in pulsatile motion.
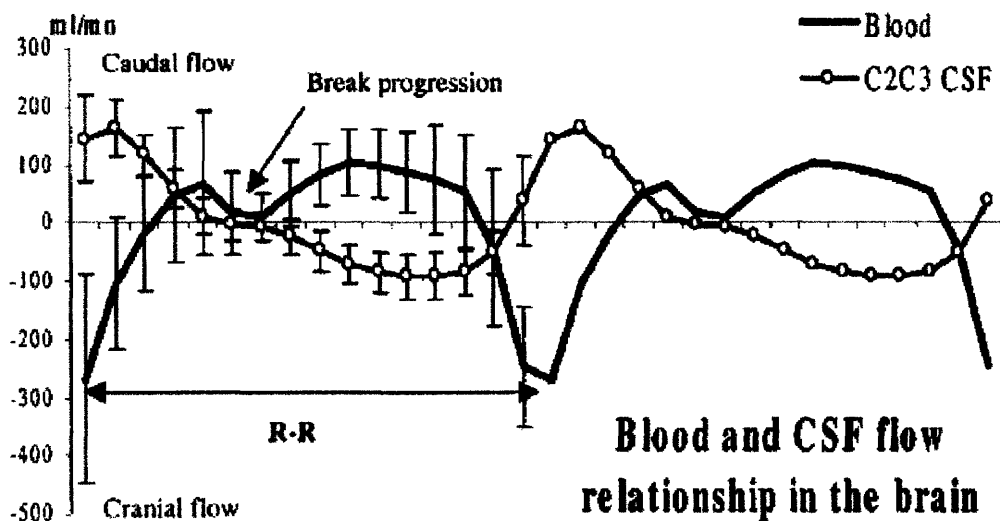
Fig. 4.13: Blood and CSF relation. The arteriovenous flow is compared against the CSF between C2-C3. Reproduced from Baledent et al.[23]

The results of both the volume graphs and the velocity graph show a clear correlation between the volume of the CSF and the blood. The direction of the velocity of the inflowing blood is opposite in direction to the velocity of the CSF. Flowing blood through the arteries has a higher velocity peak than the CSF peak, see Table 4.1 and Table 4.2. Considering the blood is traveling through smaller diameter vessels, it is going to have a higher velocity, than the CSF which is pushing through the foramen of Magnum which is a large opening that surrounds the spinal cord.

Baledent et al. [23] reported the following velocities for their research.

TABLE 1. Amplitude and Temporal Analysis of Blood Flow

	Internal carotid		Vertebral		Jugular	
	Right	Left	Right	Left	Right	Left
n	16	16	16	16	13	13
Mean flow (mL/min)*	249 ± 54	235 ± 45	97 ± 60	105 ± 43	272 ± 195	169 ± 107
T systolic (%)	0	0	−1 ± 4	−2 ± 2	20 ± 12	
Systolic peak flow (mL/min)*	384 ± 79	360 ± 73	163 ± 102	179 ± 30	372 ± 227	231 ± 124
T diastolic (%)	82 ± 2	81 ± 4	77 ± 5	80 ± 3	84 ± 12	
Diastolic peak flow (mL/min)*	173 ± 43	158 ± 73	62 ± 41	65 ± 30	197 ± 136	120 ± 88
Area (mm²)	19 ± 5	17 ± 5	13 ± 7	14 ± 6	34 ± 19	24 ± 9

n indicates number of measurements.
* Averaged over the cardiac cycle.
† Delay to the internal carotid systolic peak as a percentage of the cardiac cycle.

Table 4.1 Blood Flow velocity. Reproduced from [23]

TABLE 2. Amplitude and Temporal Analysis of Cerebrospinal Fluid and Arteriovenous (AV) Flow

	C2C3	V4 outflow	Aqueduct	V3	Monro		AV
n	16	7	16	7	18	16	n
T flush (%)†	5 ± 3	11 ± 9	21 ± 7	21 ± 6	25 ± 6	0	T systole
Flush peak flow (mL/min)*	173 ± 59	12 ± 11	13 ± 5	8 ± 3	5 ± 2.7	332 ± 108	Systolic peak flow*
T fill (%)†	70 ± 10	80 ± 8	88 ± 3	93 ± 10	91 ± 5	62 ± 26	T diastole
Fill peak flow (mL/min)*	101 ± 37	8 ± 4	13 ± 7	9 ± 4	4.2 ± 2.6	182 ± 50	Diastolic peak flow*
Onset flush (%)†	92 ± 2	96 ± 4	2 ± 3	7 ± 7	5 ± 4	87 ± 9	Onset systole†
End flush (%)†	32 ± 10	42 ± 17	56 ± 4	57 ± 9	57 ± 8	23 ± 9	End systole†
Flush duration (%)	40 ± 10	46 ± 14	53 ± 2	50 ± 5	51 ± 8	36 ± 9	Systolic duration
Stroke volume (v · mL/ cardiac cycle)	467 ± 147	27 ± 16	51 ± 25	30 ± 18	16 ± 10	800 ± 200	Stroke volume
Area (mm²)	102 ± 32	20 ± 9	8 ± 2	15 ± 4	11 ± 5		

Table 4.2 Cerebrospinal Fluid flow. Reproduced from [23]

4.6 Spinal Column

The largest CSF velocity and tissue displacement is recorded in the brainstem and spinal cord. The CSF rushes out of the subarachoid space, through the foramen of Magnum into the spinal column.
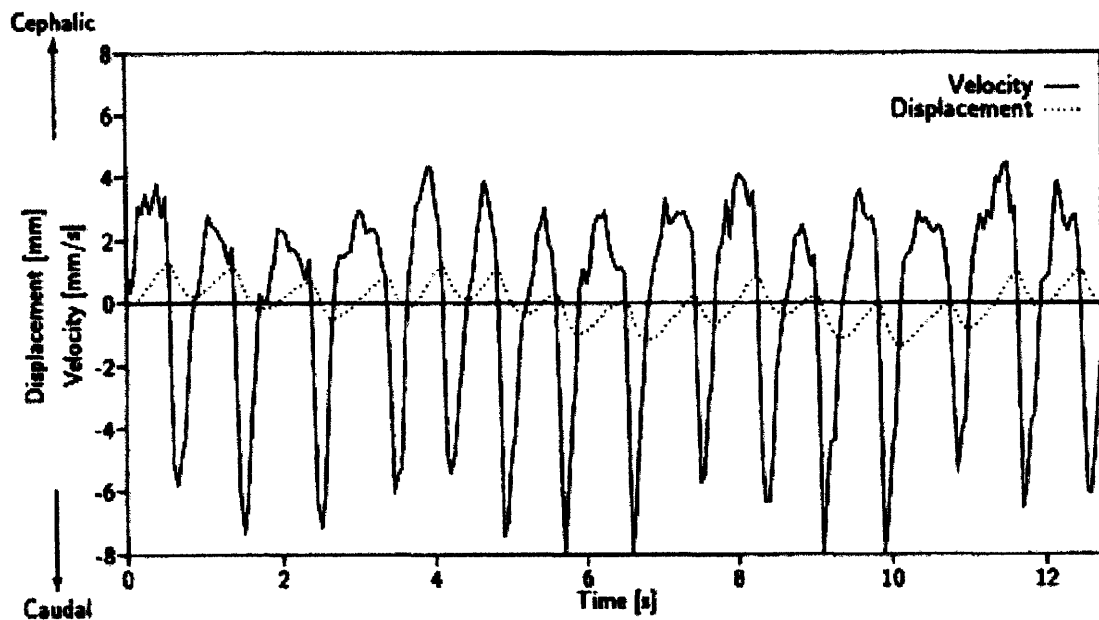
Fig. 4.14: Brainstem movement as a function of time. Reproduced from Maier et al. [20].

The velocity peak is sharper and stronger in the caudal direction. This is due to the initial strong pulsation of the carotid artery, and the fast outward flow of the CSF into the spinal column. The velocity in the cephalic direction is of longer duration and less extreme. CSF flows back into the subarachoid space in a less violent manner. The slight periodic variation in the displacement and velocity is most likely due to respiration. Respiration will be looked at later in this chapter.

4.7 Cephalic and Caudal (Up and Down) Flow

Displacement in the brain has important implications for the application of the perfusion probe. Much of the literature shows a very clear depiction of how the brain is moving. Although there are not specific locations, the overall trend is seen.
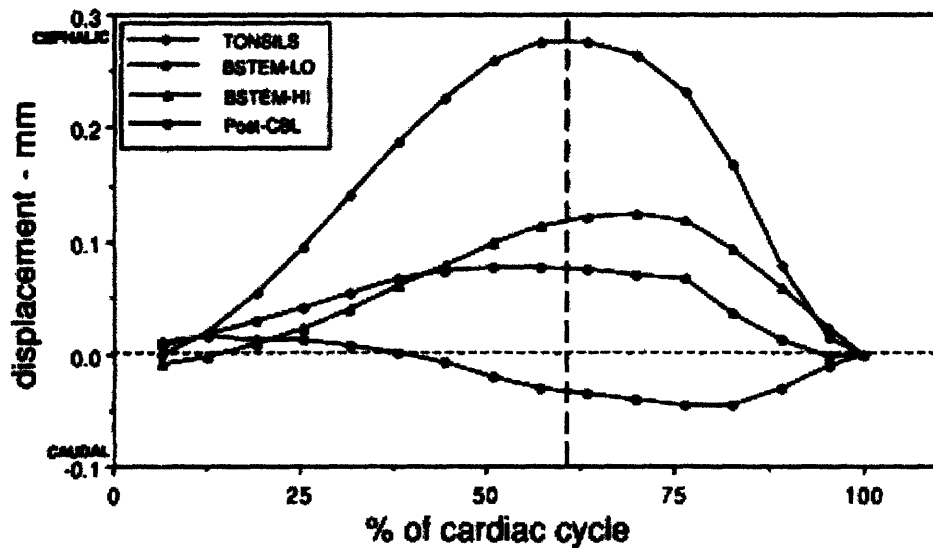
Fig. 4.15: Displacement in the Tonsils, Upper/Lower Brainstem, and Posterior Cerebellum. The cardiac cycle is defined by a peripheral trigger, putting the carotid systole at 62% or where the dotted line is present. Reproduced from Enzmann et al. [18].

At the onset of carotid systole, there is a downward displacement of the brainstem and cerebral tonsils, and an upward motion of the posterior cerebellum. This corresponds with the theory that the brainstem is moving downward while other parts of the brain are moving upward.
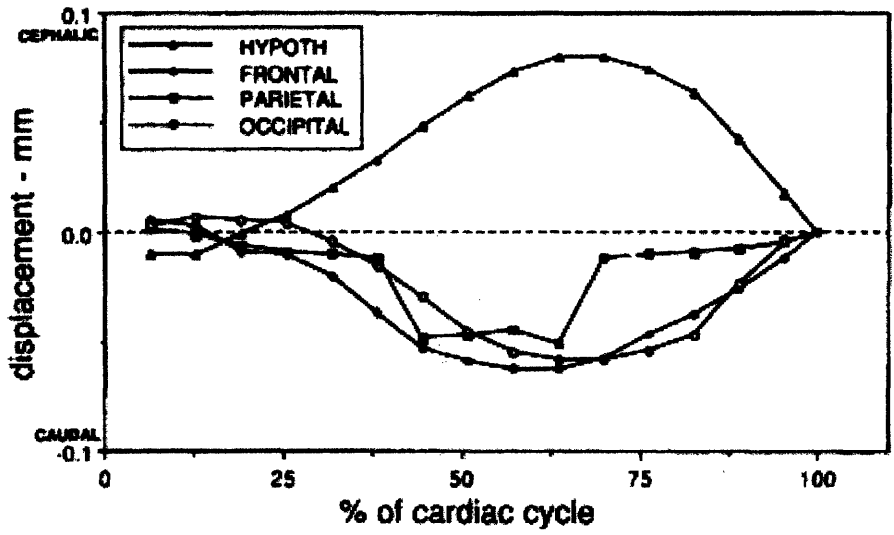
Fig. 4.16: Displacement of the Hypothalums, Frontal, Pariental, and Occipital lobes.

Reproduced from Enzmann et al.[18]

The cerebral lobes of the brain offer three dimensional analysis of the motion. They are

defined as follows.

Cerebral lobe movement is important in assessing how the brain is going to move relative to the skull throughout the cardiac cycle. At the onset of carotid systole, 62% on the graph, there is a upward or cephalic motion. This relates to the expansion of the brain with blood. More quantitatively, Enzmann et al. [18] recoded the following velocity and displacements.

Table 1
Brain Motion during Systole

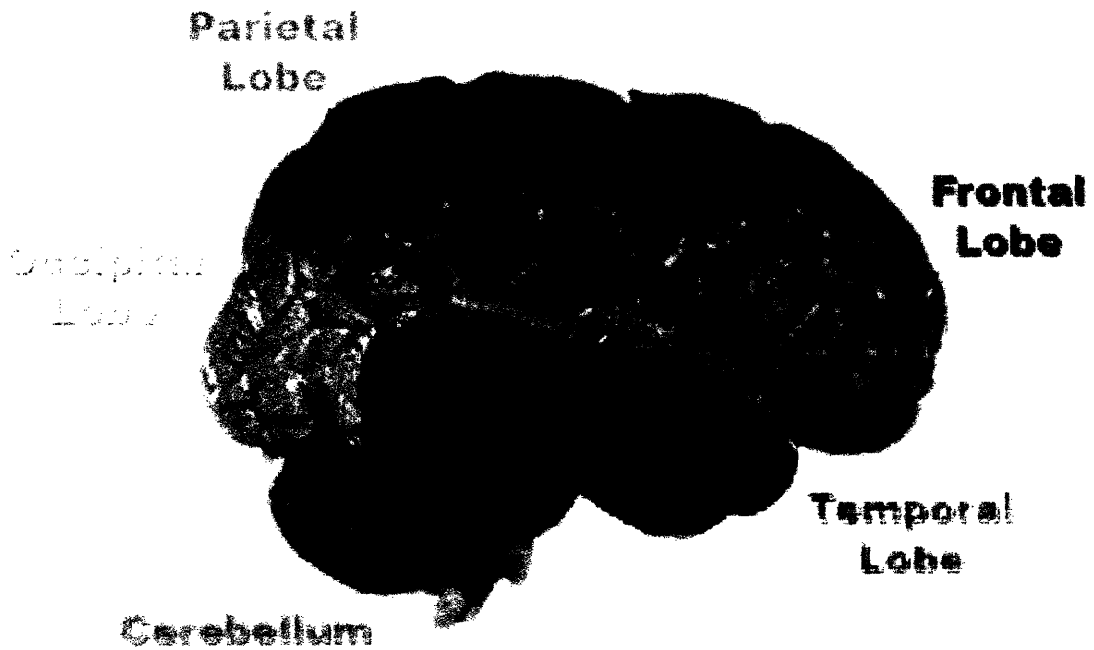| Caudal Motion	Displacement (mm)	Peak Velocity (mm/sec)	No. of Subjects
Hypothalamus	0.12 ± 0.02	1.1 ± 0.02	10
Brain stem-mesencephalon	0.16 ± 0.02	1.5 ± 0.02	10
Brain stem-medulla	0.14 ± 0.03	1.5 ± 0.03	10
Cerebellar tonsils	0.40 ± 0.16	4.8 ± 2.9	10
Cord	0.22 ± 0.06	5.7 ± 2.8	10

Note.—Values are expressed as the mean ± standard error of the mean.

Table 4.3: Brain Motion. Reproduced from Enzmann et al. [18].

Table 2
Brain Motion during Systole

Cephalic Motion	Displacement (mm)	Peak Velocity (mm/sec)	No. of Subjects
Frontal lobe	0.09 ± .02	1.1 ± 0.14	10
Parietal lobe	0.04 ± .01	0.65 ± 0.11	10
Occipital lobe	0.09 ± .03	1.2 ± 0.23	10
Posterior cerebellum	0.08 ± .02	1.2 ± 0.23	10

Note.—Values are expressed as the mean ± standard error of the mean.

Table 4.4: Brain Motion. Reproduced from Enzmann et al. [18].

Overall displacement of the cerebral lobes is below 0.1mm, with velocities lower than 1.5mm/sec. Conversely, the motion of the brainstem and lower brain structures is much greater, and the velocity is higher.
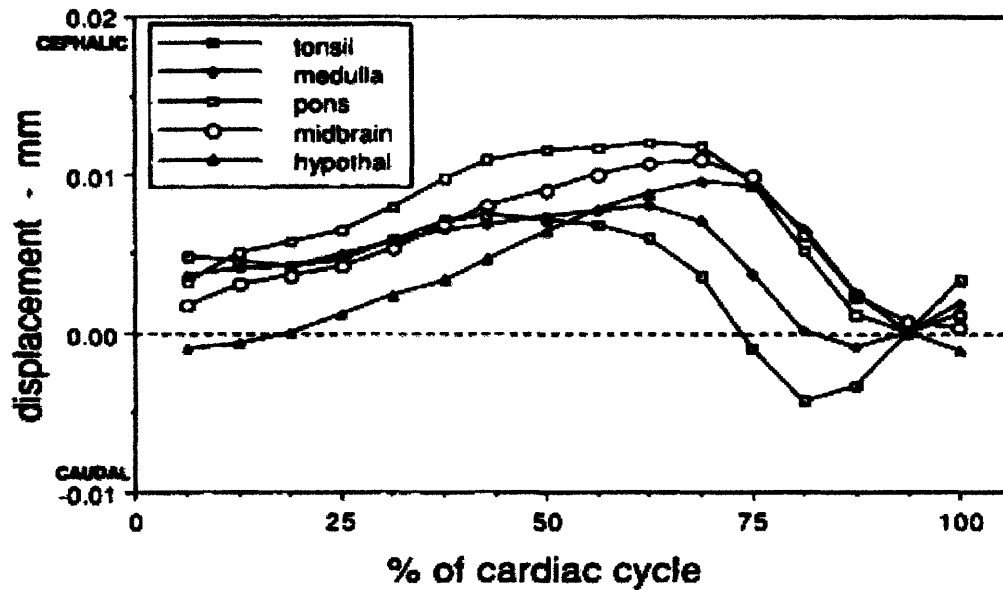
Fig. 4.17: Displacement of brain structures. Reproduced from Enzmann et al. [18].

This figure represents another depiction of the movement of the lower brain structures. A caudal motion is clear at the onset of carotid systole at 62%.

4.7.1 Time after the R wave

For a better quantitative analysis of the brain motion, it is important to be able to recognize the relation between brain motion and an overall physiological standard. This is typically the R-wave, as it is the most prominent on healthy EKG, and corresponds very closely with the beginning of the carotid systole.
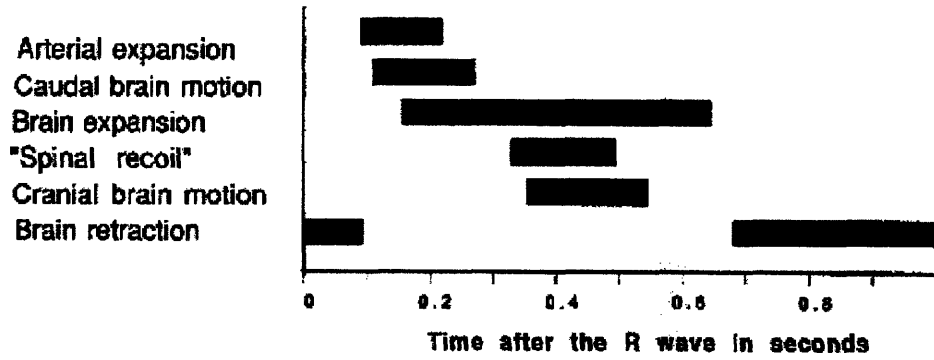
Fig. 4.18: Bar diagram of the physiological occurrences following the R-wave.

Reproduced from Greitz et al. [17].

This figure is important in understand the motion in the brain following the R-wave. It is

a helpful qualitative schematic for comparison.

b

Velocity — Caudal direction [mm/s]

Time after the R wave [s]   (RR-interval = 1.2 sec.)

c

Cranial direction [mm/s]

Time after the R wave [s]

- 72 -
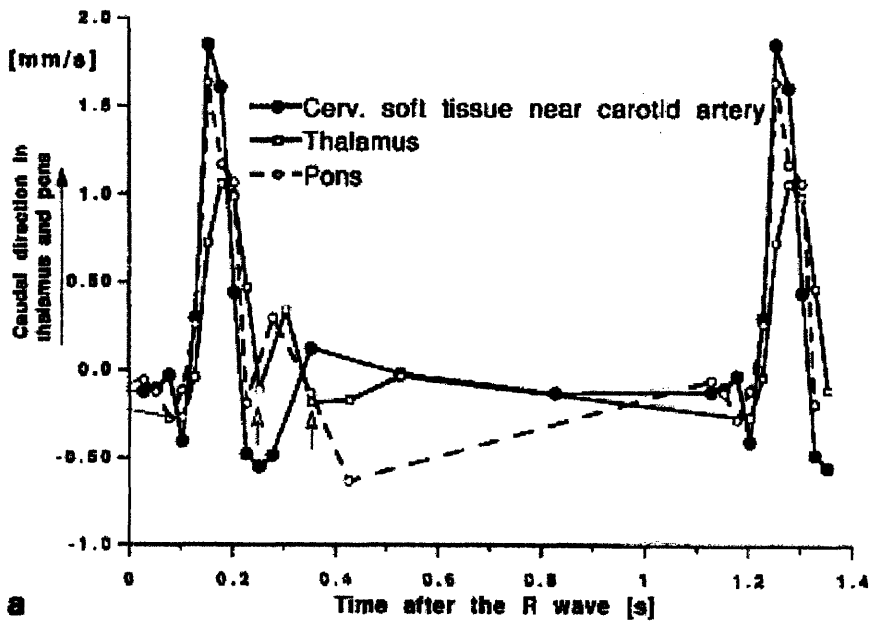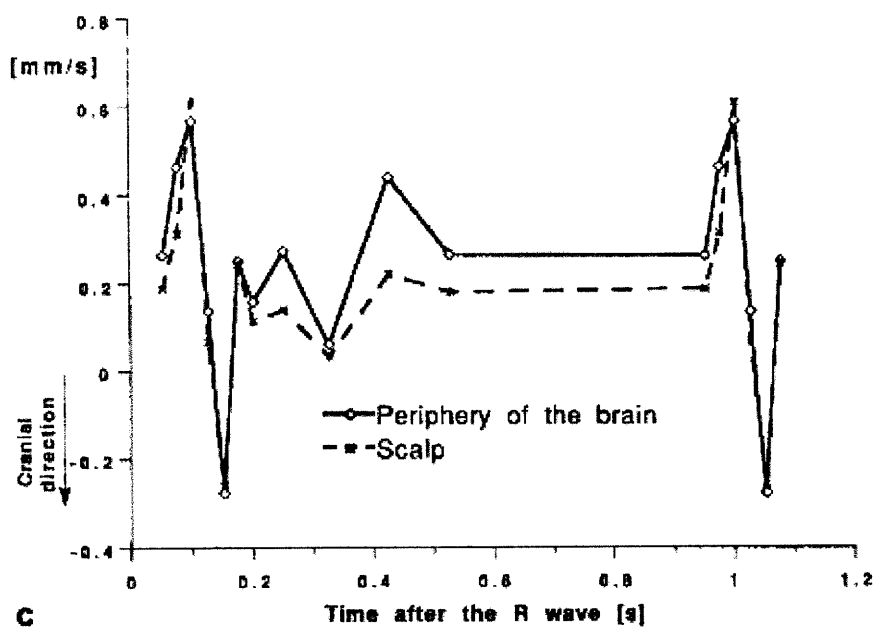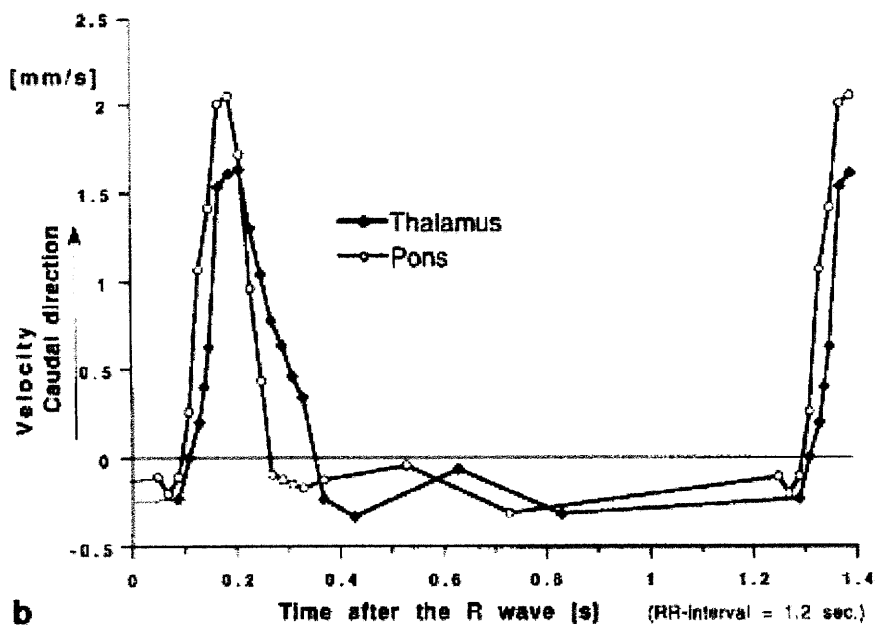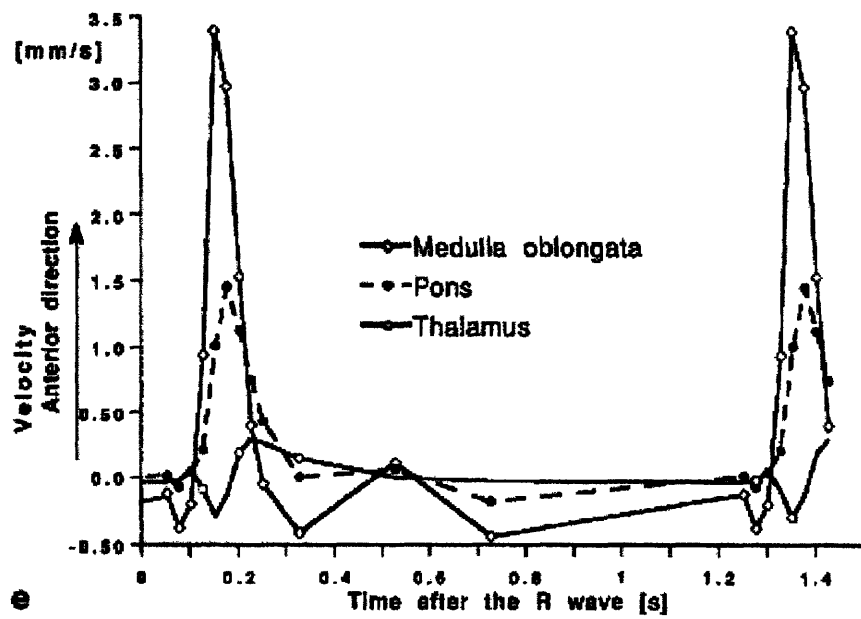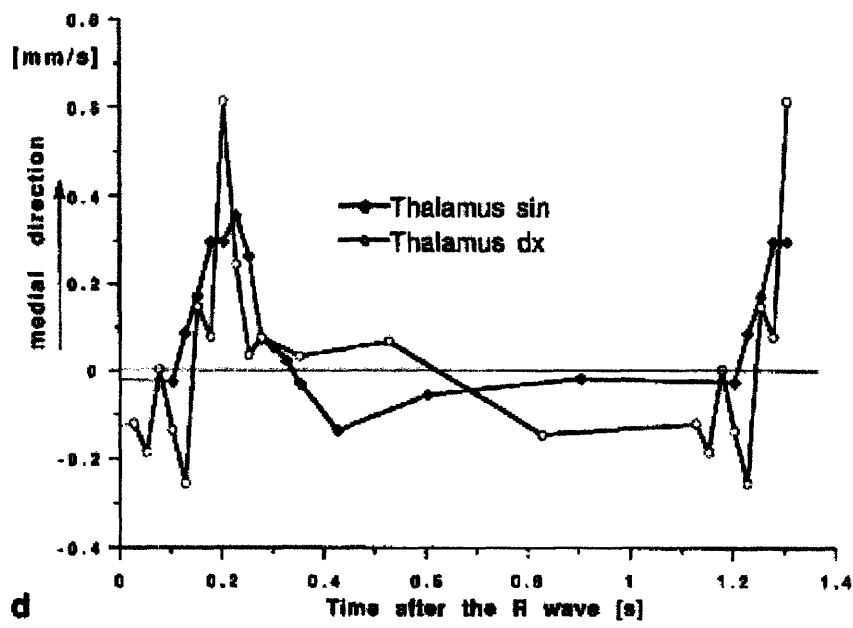
Fig. 4.19 a-e: Velocity of anatomical locations as a function of the cardiac cycle following the R-wave. Reproduced from Greitz et al. [17].

After the R-wave there is a sharp increase in velocity in most locations. This is due to the influx of cerebral blood, and the corresponding caudal motion. Most of the locations

studied are in the lower part of the brain, including parts of the brain stem. Thus, sharp

tissue velocities would be expected. The important information that is displayed here is

that different locations have different peak times. Yet, they all have relatively similar

curves. Graph c is the only one that looks differently. It shows that the scalp, or the

bone, is moving during the cardiac cycle. Considering this is physiologically impossible,

Greitz et al. [17] proposed that it is artifact at the edges of the image data.
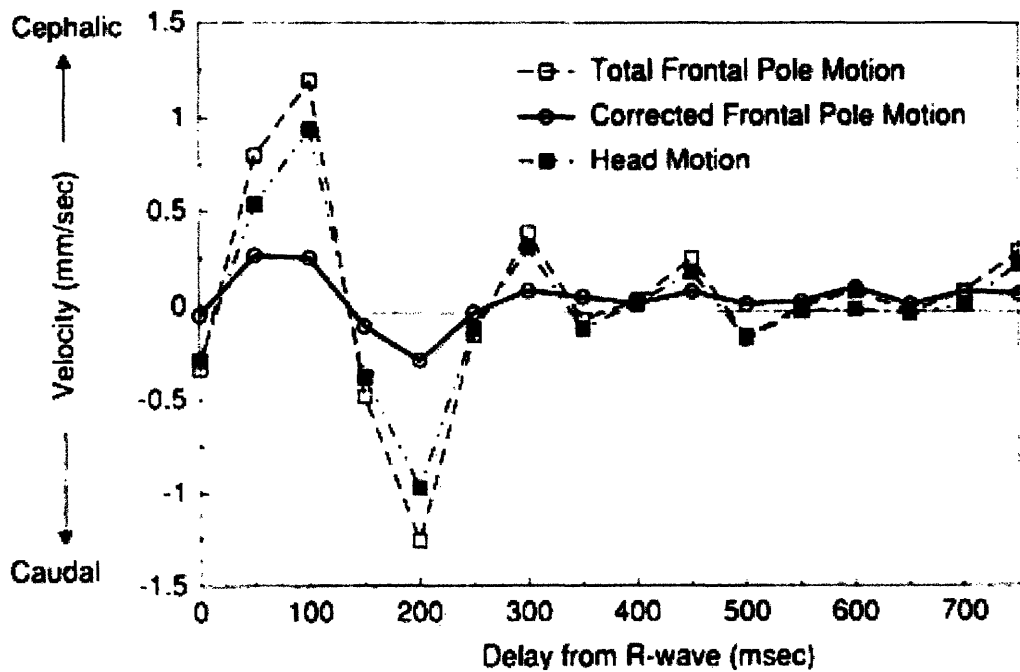
Fig. 4.20: Motion of the frontal part of the brain. Reproduced from Poncelet et al. [19].

The overall curve of the corrected frontal motion in Fig. 4.20 suggests a wave that shows

signs of damping. It has been suggested by Poncelet [19] and Greitz [17][21] that the

CSF and the spinal dural components act as a damping mechanism to the piston-like

motion of the brain and spinal cord.
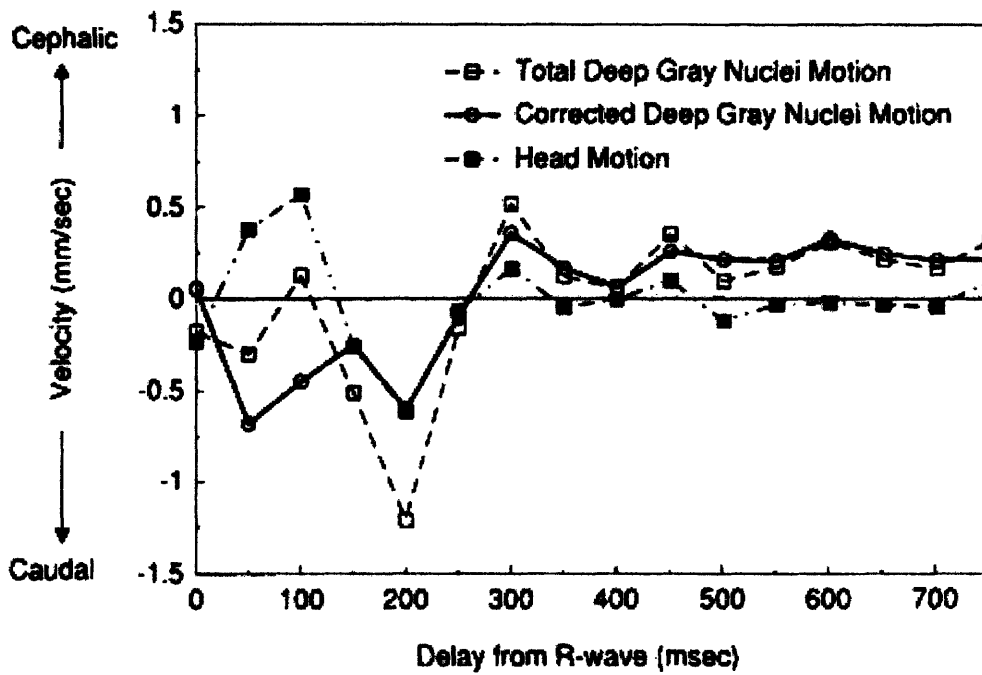
Fig. 4.21: Motion of the Gray Nuclei. Reproduced from Poncelet et al. [19].

Poncelet et al. [19] study the movement of the bulk brain tissue. Figure 4.21 again

suggests a damping mechanism on the bulk tissue of the brain.

4.8 Three-Dimensional Motion

Studying the motion of the brain using MR is done on two-dimensional planes. When all

the different axes of information are put together, a 3-D model can be derived.

Considering the brain is a 3-D object, motion in each direction is correlated with the other

directions.
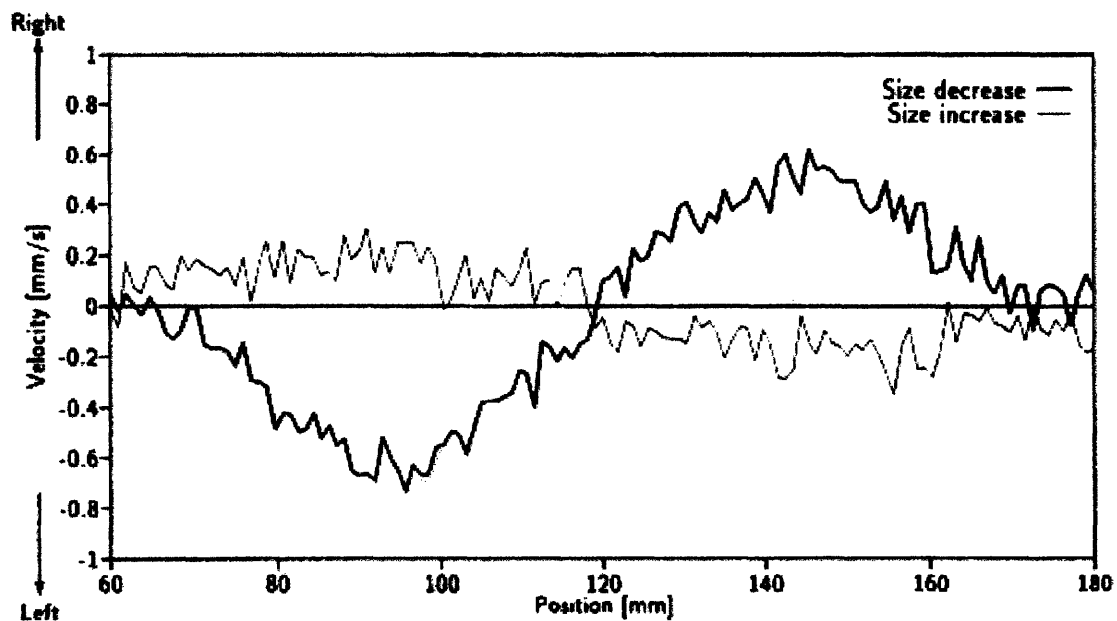
Fig. 4.22: Left and right velocity of the ventricles as a function of their position.

Reproduced from Maier et al. [20].

Deep inside the brain, the ventricles expand and contract in a left-right motion. Fig 4.22

depicts the velocity as a function of the position of the ventricles. The zero velocity

corresponds to the middle of the brain, between both ventricles. The left of the 120mm

position corresponds to the left ventricle, which shows leftward velocity profiles. The

opposite is seen on the right side. The expanding ventricles also cause the brain surrounding the ventricles to expand, which correlates to a left-right motion of the brain tissue.
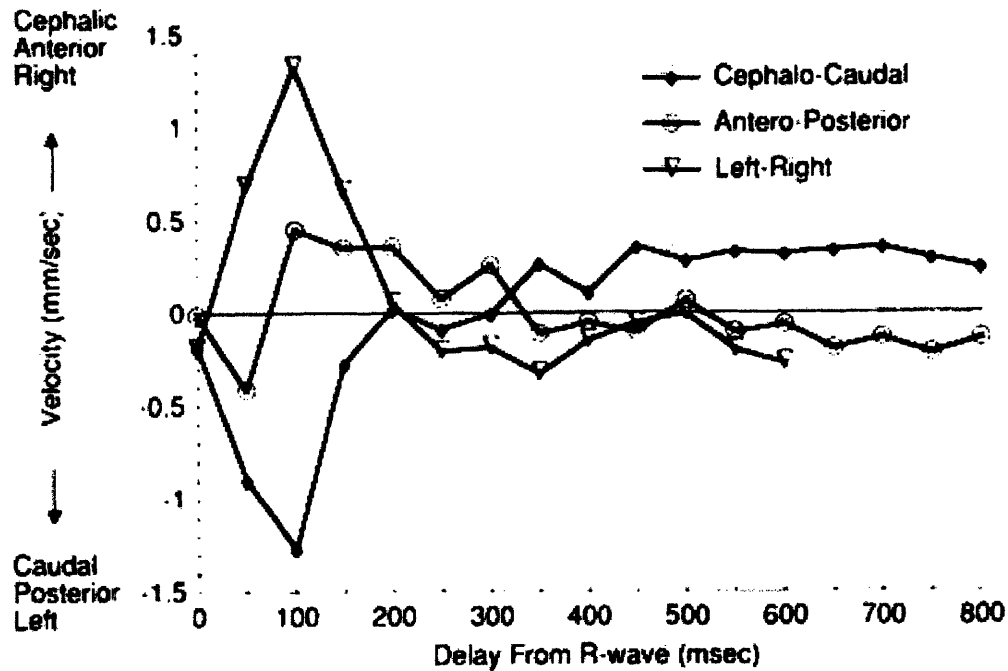
Fig. 4.23: Velocity profiles in three directions after the R-wave as seen in the 3rd ventricle through the thalamus. Reproduced from Poncelet et al. [19].

Poncelet et al., [19] graphed a three dimensional analysis of the brain motion as a function of the cardiac cycle. The three brain directions depicted have a similar shape; after a certain R-wave delay, there is a sharp peak that dissipates almost as sharply. Fig. 4.23 shows that the brain is moving in a 3-D way during the cardiac cycle. Table 4.4 is the quantitative velocities found from this study.

Table 2
Three-dimensional Brain Parenchymal Peak Velocities

Regions of Interest	Velocity (mm/sec)		
	Cephalocaudal ($n = 6$)	Mediolateral ($n = 3$)	Antero-posterior ($n = 2$)
Frontal lobe	0.29 ± 0.10	0.07 ± 0.03	0.09 ± 0.07
Occipital lobe	0.26 ± 0.10	0.11 ± 0.05	0.12 ± 0.03
Deep gray matter	0.91 ± 0.32	0.59 ± 0.20	0.33 ± 0.02
Corpus callosum, anterior	0.49 ± 0.28	0.16 ± 0.07	0.17 ± 0.04
Corpus callosum, posterior	0.36 ± 0.16	0.22 ± 0.11	0.15 ± 0.07

Table 4.5: Velocity found by Poncelet et al. Reproduced from Poncelet et al. [19].

The velocities of the upper cerebral lobes have a slower velocity than the deep gray matter, and the corpus callosum, which is the material that connects the two hemispheres. The velocity results from Poncelet, et al. [19] are lower than the velocities found by Enzmann et al. [18] as depicted in Table 4.3 and Table 4.4. A comparison of the results of the frontal and occipital lobe velocities show a discrepancy between both experiments. One suggestion is that Poncelet [19] was able to break apart the velocity into three different motions, while Enzmann [18] only accounted for a caudal-cephalic motion. Thus, there might have been more artifact in the result.

4.9 Respiration

The cardiovascular system is not the only biological system that affects the motion of the brain. Clinical data clearly reveals that respiration also has an affect on the motion of the brain. Fig. 4.14 shows oscillatory motion consisting of at least two frequencies, one corresponding to the heart rate and the other has a frequency consistent with respiration.
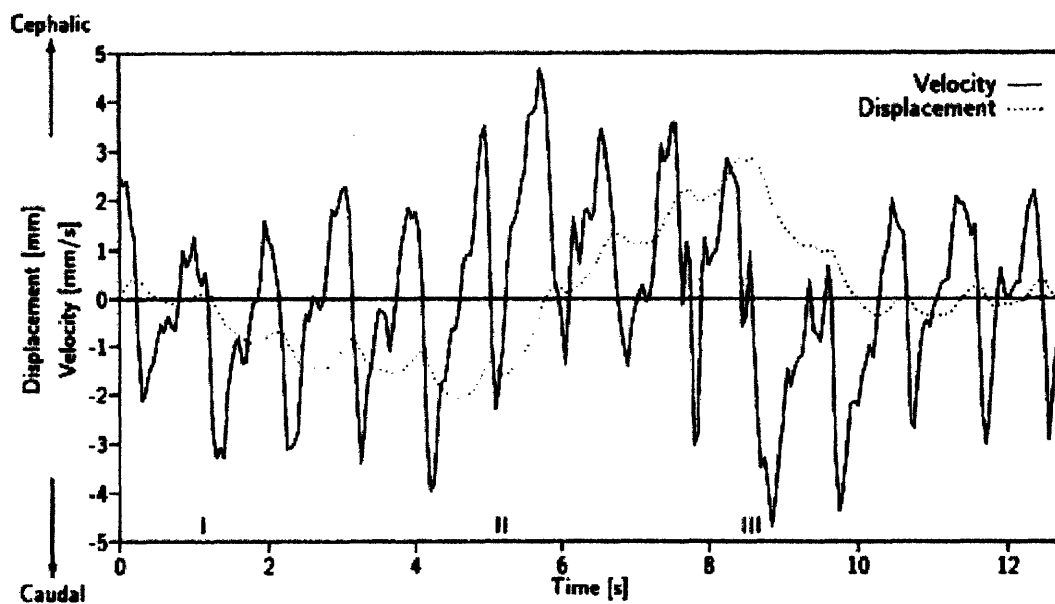
Fig. 4.24: Brain stem displacement and flow velocity showing respiration. Reproduced from Maier et al. [20].

I – Forced inspiration

II – Equilibration

III – Exhalation

According to Maier, et al., [20] inspiration initially increases venous and arterial pressures, which causes a caudal displacement of the brainstem. The arterial pressure

ultimately drops with the decreasing flow of the venous system, leading to a cranial displacement of the brainstem. At expiration, the brain stem moves back to its original position. Clinical applications of the TDP in human brains show motion induced artifact with both cardiac and respiratory frequencies. Respiratory induced motion appears to be of lower magnitude and the mechanism of how respiration influences brain motion, while not fully understood, appears to be coupled via vessel flow rate.

4.10 Cerebral Blood and CSF Flow Models

Research groups have constructed computational models for the movement of the cerebrospinal fluid. Egnor et al., [27] proposed that the oscillations of the brain and CSF can be mathematically modeled like an alternating current electrical circuit. They suggest that the CSF acts as a pulsation absorber, and thus can be modeled mathematically like a damped system. [27][28][29] The arterial pulsation is the driving force behind the system, and this leads to an overall harmonic oscillatory system. Their mathematical model quantifies the flowing brain and CSF with very promising and applicable results.

Another group, Linninger et al., [30] modeled the flowing brain and CSF using the principles of fluid dynamics. They also utilized a pulsatile model, where the CSF flow is dependent upon arterial pulsations. The validation of their model, as well as Egnor's model, provides evidence that computational models are feasible and can be accurately constructed.

Chapter 5 MR Perfusion Probe Considerations

5.1 Introduction to Probe Considerations

The medical field has seen increasing usage of medical devices in an MR environment. In order for devices to be used, they have to be compatible with and safe within the field. For the perfusion probe, MR compatibility and safety is extremely important in terms of the probe not altering the image and the EM fields not imposing artifact on the probe measurement or unduly heating the probe with eddy currents. Aside from compatibility and safety issues, an assessment of the materials has to be made to determine where problems will arise in the fabrication and implementation of the probe.

5.2 MR Compatible and Safe

The MR environment is defined as the region surrounding the MR scanner where the field strength exceeds a certain level, and is usually limited to the procedure room and inside the magnet itself. If the strength of the magnet is such that the limit threshold projects beyond the procedure room, the MR environment refers to the area within the safe field exposure lines. Field strength's below 5 gauss are considered safe to the general public. [40]

The term "MR Safe" means that the device can be used in an MR environment without affecting the patient. Being MR Safe has no bearing on whether the output of the

diagnostic data is correct, only that the patient is not harmed. MR compatibility requires the device to be used safely within an MR environment, and the device has to be able to perform its operations without decreasing the quality of the information.

There are two classes of medical devices used in an MR environment. The first is a passive device which operates without the use of any power. This includes shunts, scalpels, oxygen tanks, etc. The second is an active device that needs a power supply to perform its intended function. A power supply can be electric, battery, or gas power. Examples of active devices include pace makers, ventilators, and any monitoring system. Each of these types of devices presents their own MR constraints, and it is important to differentiate them for future discussion.

Magnetic fields, both static and time varying, have an affect on a device with a magnetic susceptibility. There are a few aspects that need to be evaluated to determine the compatibility of a device in an MR environment. The main considerations are device movement, heating, induced currents, image artifact, and device operations. Each of these constraints will be detailed.

5.3 Susceptibility

Inherently, every material will interact with and distort a magnetic field in a specific way; this is called the magnetic susceptibility, χ. [40] Magnetic susceptibility is the source of the following disturbances and lays the ground work for compatibility. Understanding

the intrinsic susceptibility and how the environment will affect it, will help solve the problem of MR compatibility of the perfusion probe. Quantitatively it is defined as a ratio of the material magnetization to the applied field.

$$\chi = \frac{M}{Bo}$$

and

$$M = Mo + \chi Bo$$

where :

$\chi = Susceptibility$

$M = Material\ Magnetization$

$Mo = Inherent\ Material\ Magnetization$

$Bo = Applied\ Magnetic\ Field$

A material may have an inherent magnetization that is present without the magnetic field, Mo. All materials, in the presence of an applied magnetic field, have an induced magnetization as defined by χBo. Thus, to obtain the overall material magnetization both of these properties need to be added. Depending on the specific susceptibility of a material, the localized magnetic field will change. Meaning that at the interface of different materials the frequency signal will be different. This is how magnetic resonance imaging is able to accurately detect different tissues. For example, the susceptibilities between bone and soft tissue are different, and exploiting this difference provides images that depict the different tissue types.

SUSCEPTIBILITY SPECTRUM
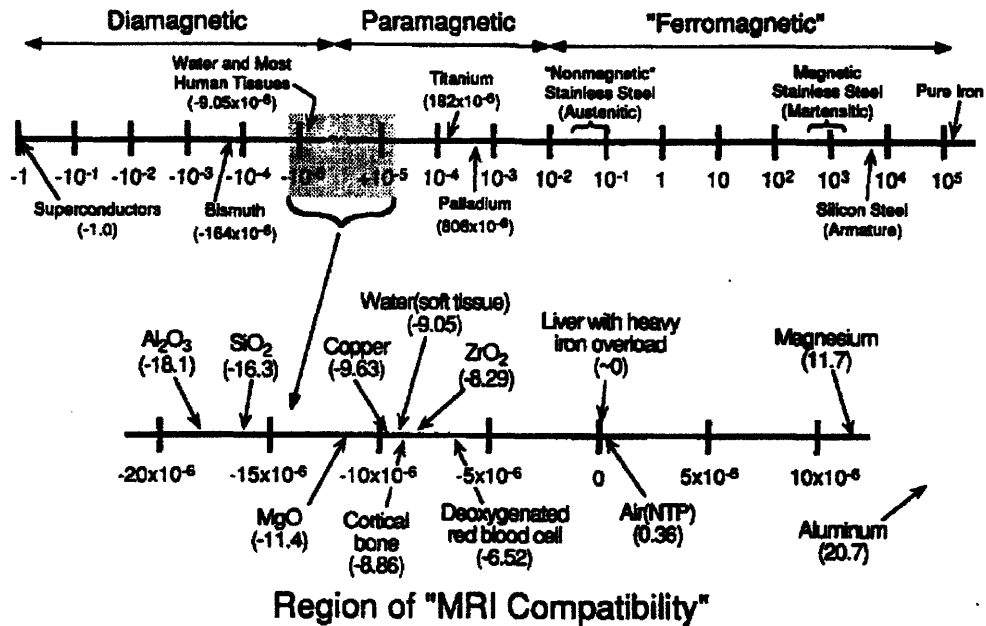
Fig 5.1. A susceptibility spectrum showing the relative susceptibilities of different materials. Reproduced with permission from Schenck[40].

Tissue susceptibilities are very small compared with non-tissue material. Thus, implanted or intraoperative devices will cause a much more significant alteration of the localized magnetic field. Most specifically, the localized magnetic field is going to change due to the different susceptibilities. To determine how a device will affect the field, there are a few aspects that need to be considered. First, the susceptibility of the material needs to be considered, then the geometry of the material, and finally how it is aligned in the field. Susceptibility is inherent, and can only be calculated experimentally. The geometry plays an important role in how the field is affected around the device. Each geometry has specific considerations, and even though most devices are

not perfectly shaped, a simple geometry is chosen to determine how exactly the geometry changes the field. Finally, the alignment is important, both in determining how the magnetic field changes around the device, and how the device will move in the field.

The geometry of a device plays a very important role in determining how the material within the device will be affected inside a magnet. For the thermal diffusion probe, there are two geometric components. First there are the heat and sense beads, which will be approximated to represent spheres. Then there are the lead wires that ascend from the beads to the monitoring equipment. The lead wires can be assumed to be cylindrically shaped.

To best approximate the thermistor, the simple geometry chosen is a sphere with radius, a. [40]

$$B_{total} = Bo + \Delta B_z$$

$$\Delta B_z = \frac{\Delta \chi Bo}{3} a^3 \frac{(2z^2 - x^2)}{(z^2 + x^2)^{5/2}} + \frac{1}{3} \chi_e Bo$$

$$\Delta \chi = \chi_i - \chi_e$$

where :

$a = Radius\ of\ the\ sphere$

$x = x\ coordinate\ of\ the\ thermistor\ location$

$z = z\ coordinate\ of\ the\ thermistor\ location$

$\chi_i = Susceptibility\ of\ the\ material$

$\chi_e = Susceptibility\ of\ the\ tissue$

As determined by Schenck [40], the field perturbation for a sphere will look as such. The clove shape characterizes the affected field, where the closer to the sphere, the more the field is affected. This result was determined experimentally by Hopper et al. [45]

$$\Delta B_z = \frac{\Delta \chi B_0 a^3}{3} \frac{2z^2 - x^2}{(x^2 + z^2)^{5/2}} \quad \text{or,}$$

$$\Delta B_z = \frac{\Delta \chi B_0}{3} \left(\frac{a}{r}\right)^3 (3\cos^2\theta - 1)$$
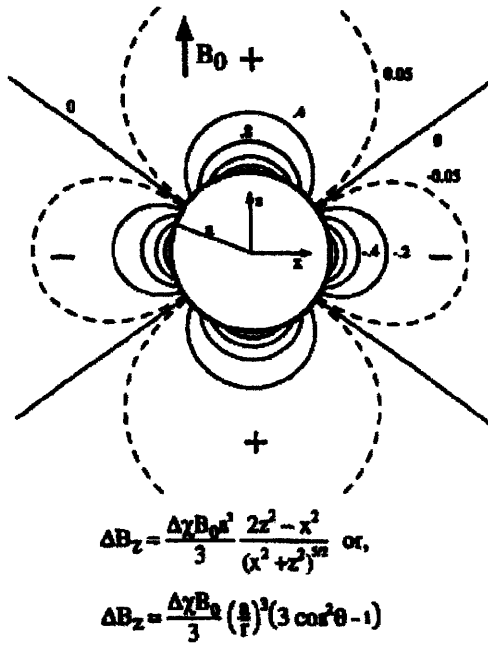
Fig. 5.2: A mathematical diagram of the magnetic field as determined by Schenck. Reproduced with permission from Schenck [40].
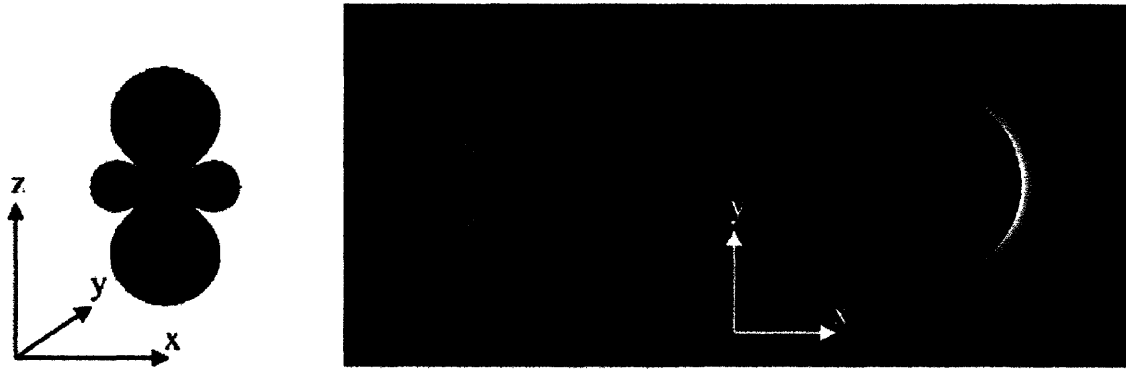
Fig. 5.3: Computer generated model, and actual artifact from a solid steel sphere. The picture shows both theoretical and experimental data. The left picture represents the computer generated model. The center is the actual image recorded, and the picture on the right is imaged on the same plane as the static magnetic field. Reproduced from Hopper et al. [45]

The second component of the thermistor that needs to be analyzed is the lead wires. A rod shape is assumed to represent the wires of the catheter. Again, the static magnetic field will be perturbed by the susceptibility of the metal wires. [46]

$$B_z^{static} = Bo + \frac{Bo\chi R^2}{4}\left(\frac{z-z_t}{\left[x^2+y^2+(z-z_t)^2\right]^{3/2}} - \frac{z-z_b}{\left[x^2+y^2+(z-z_b)^2\right]^{3/2}}\right)$$

where :

R = Radius of the bar

z_t = z coordinate of the top of the bar

z_b = z coordinate of the bottom of the bar

It was found by Bennett et al., [46] that there is more than one reason for field perturbations. Initially it was thought that susceptibility played the major role in creating artifacts. It was determined that with materials of large susceptibilities, this is true. Yet, in materials with low susceptibility, the induced eddy currents create an artifact. These induced artifacts are dominant in low susceptibility materials, and in slightly higher material susceptibility there are artifacts due to both innate material susceptibility and eddy currents. For materials of very high susceptibility, the induced eddy current artifacts are negligible. In magnetic resonance, the materials used are predominately low susceptibility, and high in conductivity. Eddy currents are also more likely to exist in higher conductive material, making the artifact also have a conductivity dependence. Thus, it is important to distinguish that there are two types of artifacts, susceptibility and eddy currents.

This characteristic of materials is important for the thermistor application, as the leads of the wires are made of copper. Materials with low susceptibility and a high conductivity, like copper, will be affected significantly by eddy induced artifacts. Bennett et al. [46] proposed how the magnetic field will be changed in the presence of such materials. Eddy currents create a magnetic field that opposes the field. Thus, when a radiofrequency pulse is applied orthogonal to the static field, eddy currents decrease the strength of the applied field.

$$B_x^{rf} \approx -2xyB_{applied}^{rf}R^2(x^2 + y^2)^{-2}$$

$$B_y^{rf} \approx B_{applied}^{rf}\left[1 + R^2(x^2 - y^2)(x^2 + y^2)^{-2}\right]$$

It was discovered by Bennett et al., [46] that a four-lobe artifact is produced from the eddy currents in wires that were highly conductive, and low in susceptibility. This was compared to wires that were higher in susceptibility; they showed a circular blurring affect of the lobe artifact.

In conclusion, there will be two predominate artifacts that are created by materials inside a magnetic field. Materials with a high susceptibility will have artifacts due to the inhomogeneity of the surrounding field, while materials with low susceptibility and high conductivity will have artifacts correlated with eddy currents. With an application of a metal oxide, there is going to be inhomogeneities within the material. This could potentially cause a non-uniform artifact, and one that is case dependent.

Another aspect of induced artifact has to do with the positional errors. When there are field imhomogeneites, like the ones produced by metal objects, the position of the spins is affected. The MRI algorithm mismaps the detected signal, producing a reconstructed image that is not anatomically correct. [45][46] The readout of the object is going to have some areas that have less proton density, and others that have more proton density. Also, as a matter of later development if the thermistor is placed during an operation, there is going to be a slight positional error on the images produced in real time.

5.4 Device Movement

There are two types of movement that have to be analyzed, translational and rotational. In a three dimensional space, this corresponds to six degrees of movement. Translational movement will occur when there is a magnetic gradient present. The static field is not fully uniform due to inherent variability, and when a gradient field is used, there is an induced magnetic gradient. This can cause a translational motion that could pull the device inside the magnet. Typically, the bore of the magnet has the strongest magnetic field, and it decreases with distance from the center. An extreme example of this is when an oxygen tank is accelerated across the room straight into the magnet. On a more applicable level, a device can be accelerated by the magnetic gradient causing a tearing of the tissue.

Rotational movement occurs when a device aligns with the magnetic field. Most magnetically susceptible materials align either parallel or perpendicular to the static and applied fields. If the device does change its alignment, it will cause a torque that could cause a tearing of the tissue. Another problem regarding rotational movement is the time-varying magnetic field. If the device aligns to the static field, it could also be affected by the time varying field causing an oscillatory motion between static alignment and time-varying alignment.

With devices whose composition is not completely homogenous, the movement will be dependent on a specific area. Having a composition that has varying properties, presents

a variation of results concerning how they are affected inside a magnetic field. For example the composition of metal oxides is not completely homogeneous, so there will be certain areas of the material that will have different properties. Meaning that one side of a thermistor could have a higher metal susceptibility causing it to have a greater rotational torque.

Another aspect that causes motion is induced currents within the metal. The changing magnetic field induces a current within a resistive material. The flowing current arises in a direction that would oppose the changing magnetic field, in a way to decrease the effective change. This induced magnetic field will want to align in a position of least energy. If it is not in alignment, it will rotate to be in such an alignment. Eddy currents within an electrically conducting material cause a torque on the material.

Faraday's Law states that a changing magnetic field within a defined area will induce a current.

$$V_{IND} = \frac{d\Phi}{dt} = \frac{d(A \bullet B)}{dt} = A \bullet \frac{dB}{dt} \qquad (Eq.5.1)$$

$where:$
$V_{IND} = Induced\ Voltage$
$\Phi = Flux$
$A = Area\ of\ current\ loop$
$B = Magnetic\ Field$

This equation becomes slightly modified depending on if the area is a current loop of one or multiple turns, or a rectangular frame. Regardless of specifics, when there is an induced voltage within a resistive circuit, there will also be a current.

$$I_{EDDY} = \frac{V_{IND}}{R}$$

$(Eq\,5.2)$

$where:$

$I_{EDDY} = Eddy\,Current$

$R = Resistance$

Consequently, when the electrical current flows through the resistive material, heat is lost internally. Joule heating or ohmic heating is kinetic energy lost by the moving electrons to the atoms in the resistive material. This will ultimately cause the overall temperature of the thermistor to increase. Considering the TDP uses Joule heating in the process of determining perfusion, any induced temperature increase of the thermistor is going to cause a corresponding error in the perfusion measurement.

An applicable research study was done by Roguin et al. [44] that examined implantable cardiovascular devices, including pacemakers and implantable cardioverter/defibrillators. They specifically studied the heating of the device leads due to the magnetic field both in vitro and in vivo. The leads of cardiovascular devices are approximately the same scale as the thermistor probe leads. The study found that the end of the leads heated by 0.2°C in vivo. Thermistors used in measuring blood perfusion have an important resistance vs. temperature characteristic. If there is an outside force creating more internal heat for the thermistor, the power needed to keep the thermistor at a certain temperature is going to

depend on more than was initially calculated. Within the current computational algorithm, the power needed to maintain a certain temperature is dependent on the resistance of the thermistor material and the thermal transport properties of the tissue. With heating due to the magnetic field, the additional heat will resulting in the controller providing less heat than with absences of the magnetic field; thus providing a some what reduced value of measured perfusion.

The experimental results regarding device heating are not as conclusive as would have been helpful. Usually the incidents of heating occurred in large metal objects, like ones that would be used in MR-guided surgery. The heating of such devices was less than one degree Celsius. This is within the range for having no biological affects, but does effect the measurements derived from the probe. Also, the devices used were rather large, so size has to be taken into consideration when device heating is considered. [41]

It has been confirmed by many reports that the area of greatest heating is at the ends of lead wires. This is significant to the perfusion probe application because the lead runs right into the thermistor, which resides at the distal tip of the embedded probe. At that interface, the behavior is currently unpredictable. Also, the lead wires run from within tissue to the outside. This is going to add an additional consideration to the analysis of the lead wires.

Yeung et al. [47] proposed a method to asses the safety of implanted wires in an MRI. The safety assessment depends upon the RF heating of the wires. They found that there

are many factors that affect the heating of the wires. The diameter, length and insulation thickness all affect the RF heating. Another factor that affects safety is tissue conductivity. Considering that the perfusion probe will be in tissue of different conductivities, this is an important consideration. With increasing tissue conductivity, the safety increases. This makes theoretically sense, because perfused tissue removes the heat by convection, and the higher the level of perfusion the greater the heat removed. The results from this study are presented below.
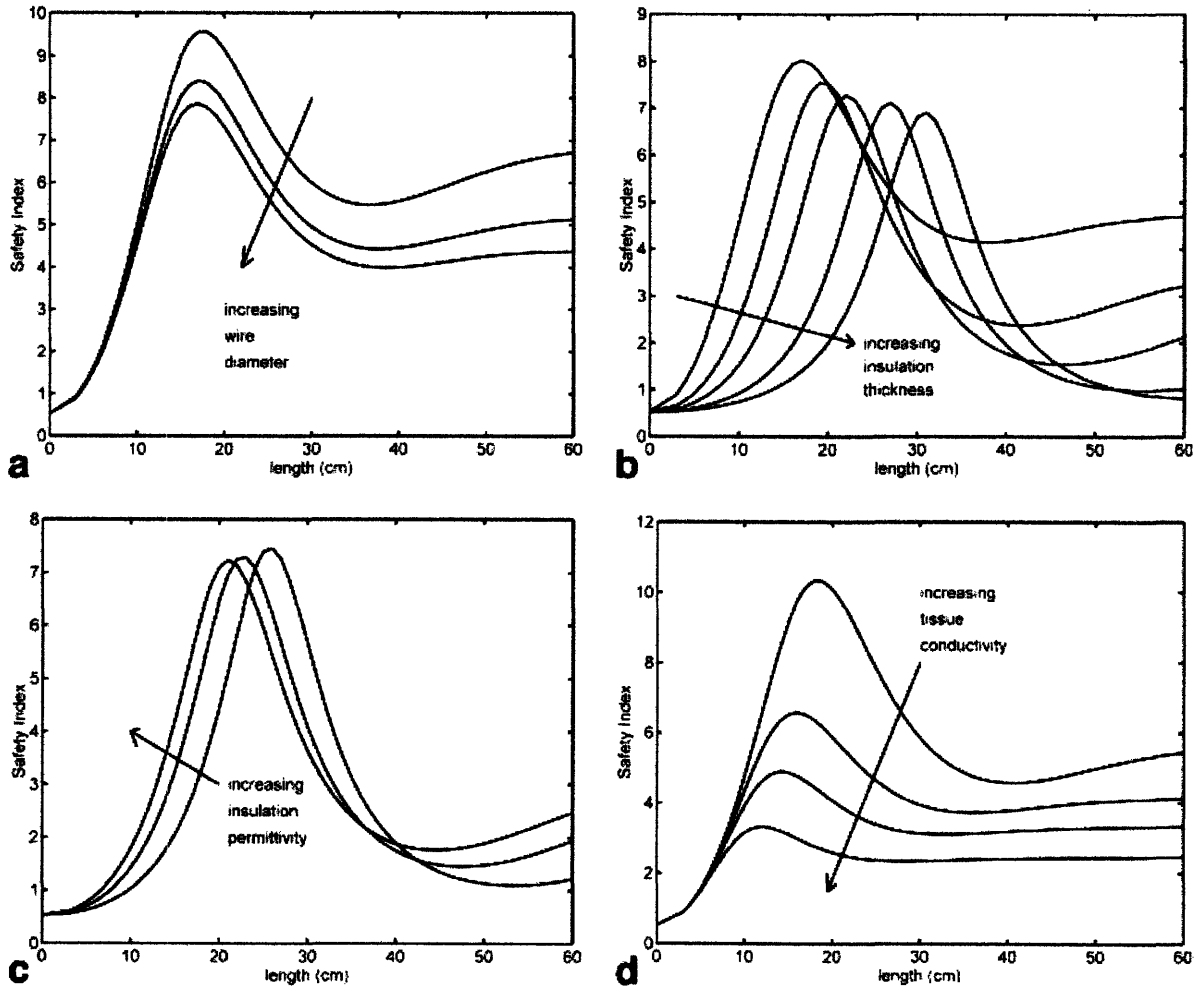
Fig. 5.4: Theoretical results of wire length vs. safety from Yueng et al., [47] for the safety of wires in an MR environment. The wire diameters in (a.) are 0.2, 0.4 and 0.8mm. The insulation thickness for part (b.) is 12, 25, 50 and 75μm. The Safety index is measured in (°C/(W/kg)).

The Safety Index can be thought of as increased heating. Although this is not a quantitative result, the general trend can provide insight into the perfusion probe application. Yueng [47] concluded that conductivity and insulation thickness have a stronger affect on heating than does the wire diameter or insulation permittivity. The

peak of the results is due to the resonance length. The right side of the curve is under the resonance length, while the left side is over. This study was only conducted on fully implanted straight wires. It cannot be directly applied to the perfusion probe, as the probe is not fully implanted. Yet, the dimensions of their analysis are important for future considerations.

5.5 Magnetoresistance

Magnetoresistance is defined as the property of a material to change their electrical resistance when exposed to a magnetic field. In metallic materials, the outermost electrons of the metals are typically mobile compared to the localized electrons used in bonding. This phenomenon explains how a material can conduct a current. Within a solid structure, there are two important electron interactions, electron-electron and electron-lattice. The relationships of these interactions dictate the behavior and properties of the material.

Certain material structures exhibit behaviors that correspond to a higher incidence of interactions between electrons and lattice-vibrations. Electrons can move to other sites temporarily affecting the crystalline structure at that site. The localized distortion can cause electrons to be stuck in the improper position. This occurrence can be large enough to greatly change the properties of the material.
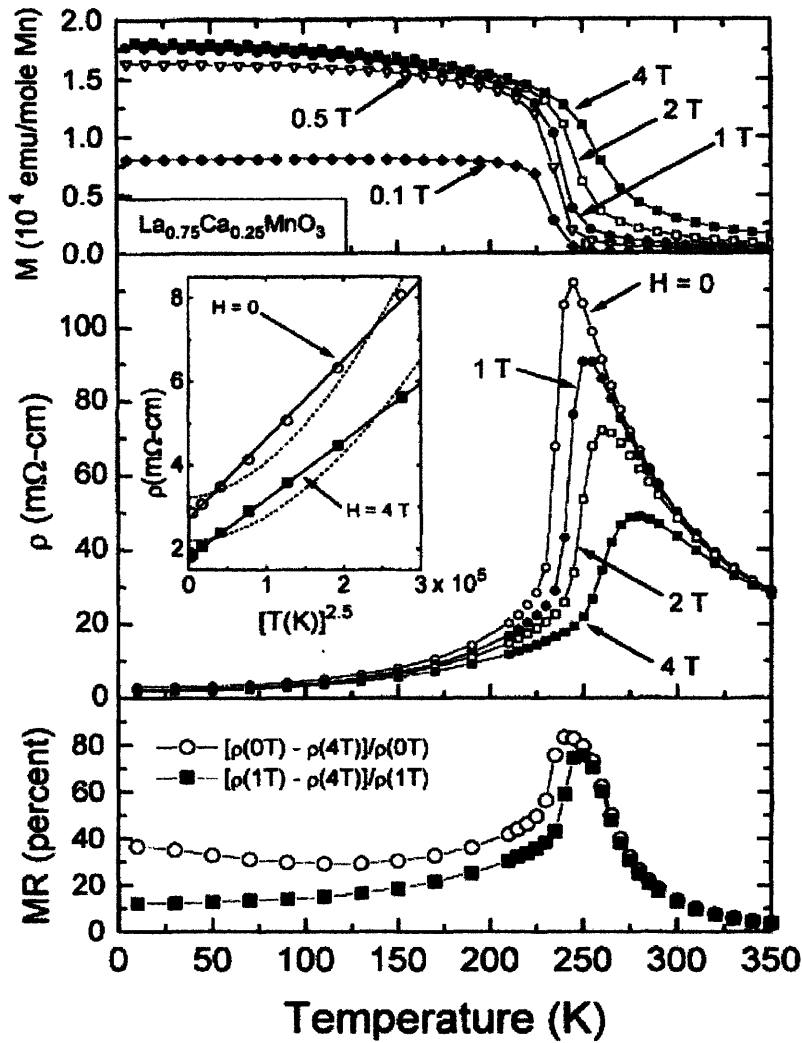
Fig 5.5: The magnetization, resistivity, and magnetoresistance of $La_{0.75}Ca_{0.25}MnO_3$ as a function of temperature. Reproduced with permission from Schiffer et al. [49].

The outermost electron shell in transition metals is filled following Hund's rule. The electrons will fill the shell in a spin-up configuration, until it is half full and then the rest of the electrons required to fill the shell will double up in a spin-down configuration. The spin-up and spin-down electrons neutralize the spin state. If a shell is completely filled then it is considered diamagnetic. In a shell that is not completely filled, there will be unpaired electrons providing an overall bias toward a certain spin state, this is called

paramagnetic. Depending on the number of electrons within the shell, the atom will have present different properties regarding magnetization.

When energy is applied to a system, the electrons can jump to a higher shell causing a shift in paramagnetic and diamagnetic features. Energy is usually added to the system in the form of heat, either through external temperature or internal Joule heating. Another occurrence with the addition of energy in a solid structure is the movement of electrons to fill charge carriers or holes. The changing of spin orientation is going to have an affect on the overall resistivity of the system. Spin disorder causes the scattering of holes with different spin orientation. The scattering increases the electrical resistivity. Within an applied magnetic field, all the unpaired electrons align with the field, hindering the scattering due to spin disorder and thus there is a loss of electrical resistivity.

Geometry also plays a role in determining how properties are going to change within a magnetic field. The orientation of the ions, and more specifically the unpaired electrons, as well as, the deformation in the lattice structure will all be affected differently depending on the direction of the magnetic field. Considering that non-coupled electrons align with the magnetic field, their orientation is important. In a magnetic resonance (MR) environment there is a constant static magnetic field. During a scan, there are two other magnetic fields present, the field produced from the rf-sequence, and the gradient. The interactions between each of these magnetic fields on the geometry are going to affect the resistances of the material.

On a more applicable level, the resistance of the metal oxide in the thermistor is going to change depending on the strength and direction of the magnetic field. In a non magnetic environment, a thermistor operates on its very material dependent and well-known resistance vs. temperature characteristics. In the particular temperature regions of interest, a thermistor used for sensing will have especially large temperature coefficient of resistivity. This also provides large sensitivity to temperatures changes in that region. Thermistors used in tissue thermal property and perfusion measurements have a negative temperature coefficient, meaning that as temperature increases, the thermistor resistance decreases. This characteristic facilitates implementation of the electric controller.

Negative temperature coefficient of resistivity (NTC) thermistors have a current bias which correlates to their ability to control Joule or resistive heating. When a current passes through a thermistor, some of the current is lost to heat due to the internal resistance of the materials; this is called Joule heating. As the thermistor increases in temperature, the resistance will decrease because of the NTC, and this will prevent additional temperature increases. The accuracy of this correlation indicates that the resistance of the thermistor and the rate of heat transport in the material can be derived by the power needed to maintain the thermistor at a specific temperature.

The resistance of a material is dependent on the material temperature as well as the strength of the applied magnetic fields. For the metal oxide represented in Fig. 5.5 there is a positive coefficient of resistivity, and a negative magnetoresistance relation. As the magnetic field increases, the resistance is less affected by increases in temperature.

5.5.1 Magnetoresistance and Doping

To obtain the large sensitivity of a thermistor over a certain temperature range, the chemical properties and dopant concentrations must be precise. There are specific compositions that will create the desired resistance vs. temperature characteristics. Often the specifics are privileged information, and only the empirically derived data is released. Typically commercially available thermistors for human body applications are made of mixed metal oxides, yet the exact composition and even the main metal component is unavailable. Even though the specific composition of the thermistors in the TDP is unknown, studying the behavior of metal oxides in general will provide the theoretical basis for understanding the behavior of these materials.

Doping of the material also accounts for different properties in a magnetic field. The concentration of certain ions will change the bonding, and positions of the electrons.
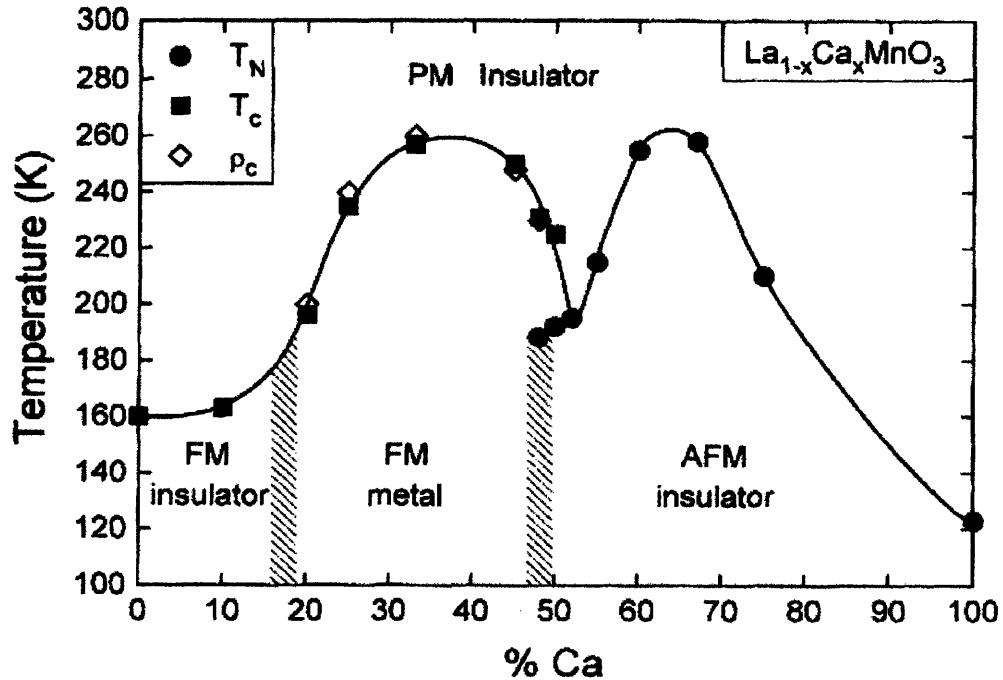
Fig. 5.6: Phase diagram of $La_{1-x}Ca_xMnO_3$ as a function of temperature and concentration. The solid line represents the approximate boundary between paramagnetic states and ferromagnetic states. Reproduced with permission from Schiffer et al. [49].

The ability of a thermistor to function in the desired manner depends on the precise resistance vs. temperature relationship. This is an innate quality of the thermistor material, and does not change in most environments. Yet, if a thermistor is placed in a magnetic field, the internal resistance is going to change. This behavioral change is going to have an adverse affect on any resistance vs. temperature algorithm written whose R.T. dependence is determined in an environment with different or no EM field. In a new EM environment an entirely new R.T. relation is needed to produce accurate results. Considering the composition of the TDP materials is unknown, the TDP thermistors have to be studied experimentally in the appropriate magnetic environment to determine the exact relationship.

Chapter 6 – Comments and Recommendations for Further Work

6.1 Introduction

The focus of this thesis is twofold; first to evaluate the factors involved in rendering the TDP MR compatible, and second to look at cardiac induced motion of the brain and the role of brain motion in TDP perfusion artifact. The data collected and compiled in this thesis offers a substantial background for both issues. While it is beyond the scope of this thesis to construct MR compatible perfusion probes or write algorithms to compensate for brain motion, recommendations are offered for next steps in the process of creating a MR compatible perfusion probe whose data can be corrected for brain motion.

6.2 Thermal Diffusion Probe Recommendations

The exact material composition of the thermistors is generally proprietary, and thus we are stuck with the electromagnetic (EM) properties they exhibit. This means that all the information regarding the thermistor is going to be experimentally determined. The analysis from chapter 5 offers a solid foundation for the considerations and tendencies that will be expected with mixed metal oxides in an MR environment. The principal challenges that will be associated with TDP use in the brain during MR images are probe heating, probe data artifact, EM induced motion, and altered magnetoresistance. If the thermistor is not self heated during a scan, only the probe heating, and image artifact are

of significance. If the thermistor is self-heated during an MR scan, in an effort the get simultaneous perfusion data, than all four factors maybe significant. The largest challenge will be the EM induced change in magnetoresistance as this will change the temperature vs. resistance relation and may significantly alter the probe calibration leading to errors in measured perfusion.

To counter the image artifact created by the TDP (a metal object), there are certain scanning sequences that can decrease the effect of such foreign objects. These scanning sequences are currently in use for patients with implanted cardiac devices or metal plates. Some resolution is lost in these images. It is a classic benefit vs. disadvantage optimization problem. For example, if real-time perfusion information is clinically more important than the resolution of an image, than the probe should be used despite some blurring of the image in the immediate location of the probe.

Probe heating is a potentially significant factor regarding the thermistor in an MR environment. Unfortunately, the only way to fully test the heating effect is to conduct controlled experiments. Many of the papers researched reported that there was no significant MR heating of metal objects where the temperature elevation went beyond a level unsafe for the patient. This is an important result for our application. Even if the thermistor is not active (as in acquiring perfusion data) during an MR scan, it can and will heat somewhat, and this heating of the thermistor must still be within a safe level for the patient. The perfusion probe is used in perfused tissue, and the presence of perfusion will greatly facilitate the removal of the MR induced probe heat. EM induced probe

motion is another factor that needs particular attention. Putting any metal device in an MR field will have a translational and/or rotational motion effect in all three axis of space. The question is whether or not these EM field induced forces produce motion that is clinically significant. Tissue will be able to handle small forces; when the forces become great enough to cause tearing or ripping, then problems will arise. Understanding if and how these EM induced forces may cause thermistor based sensor motion requires a full analysis and/or appropriately designed experimental studies.

The portion of the non MR compatible TDP that we have the most control over is the lead wires. Placing a resistive material in an MR environment causes Joule heating and an induction of its own counter magnetic field. Lead wires are essential to the TDP, thus a design consideration will be used to this effect. The primary consideration for the lead wires is the conductive properties of the materials chosen. Similarly to the thermistor; motion, heating, artifact, magnetoresistance, and an induced magnetic field due to eddy currents are lead wire design concerns. Joule heating and EM induced motion are not as significant in the lead wires as they are in the thermistor.

Lead wire factors that are within our design control include length, diameter, material, and orientation; each of which influence the ultimate perfusion data accuracy and compatibility of the lead wires. According to Figure 5.4, there is a significant dependence of the safety (temperature) on the length of the wires. At the resonance length, there is a peak that corresponds to an increased and potentially unsafe zone of high temperature. (The FDA does not permit implanted devise to operate at temperatures

above 41°C [34]). It is important that the length of the lead wires is longer than the resonance length; also, at longer lengths, many of the safety related properties come to a steady state and are less variable on length. Figure 5.4 d. shows safety (temperature) as a function of tissue perfusion; wire heating is a function of tissue perfusion. The resonance peak of Fig. 5.4d, decreases significantly with increased perfusion.

Conductive materials within an MR environment have induced eddy currents, which are moving electron currents. These moving electrons give rise not only to Joule heating, but also to their own magnetic field that acts to counter the applied magnetic field. At the regions surrounding the wire, the magnetic field will be decreased, causing artifact in the image data. When current runs in the same direction in parallel wires, they repel each other. This is due to their magnetic fields circumventing the wire, so they are opposite on each side. Eddy induced currents flow so as to decrease the strength of the static field. Thus it will be flowing in the same direction of both, but not necessarily in the direction of the wire, it will depend on the angle of the magnetic field to the wire. The angle dependence between the strength of the magnetic field felt by the wire, suggests a way to decrease the induced eddy currents by decreasing the angle. In an MRI, there are three different magnetic fields, the static field, the gradient, and the rf-pulse. Thus, it is difficult to align the wire with any of these fields. When the wire is parallel to the rf-pulse, the least artifact occurs within the image and the output data. If the wire is parallel to the static field, the least amount of joule heating will occur, as this field is always on. By varying the angle, there might also be a decrease in the eddy currents; this would be done by twisting the lead wires around each other.

6.3 Brain Motion Considerations

There is strong evidence, cited in a growing literature, of pulsatile movement of the brain that is dependent upon the cardiac cycle. The literature researched has shown a clear correlation between the movement of the flowing cerebral blood and the CSF as a function of the cardiac cycle. Motion of the brain, brainstem, and spinal cord, was investigated in terms of velocity and displacement. Brain motion has been described to move in a piston-like fashion where the influx of arterial blood into the brain, expands the brain, pushing CSF out of the subarachnoid space, through the foramen of Magnum (the opening at the base of the skull) into the spinal canal. [16] The fluid pushes down upon the elastic dura of the spinal column and eventually recoils, sending the spinal cord in a cephalic direction. The greatest overall velocity and displacement was found to be the brainstem.

Although the mechanism of how and why the brain moves within the cranium is still somewhat controversial, there is no question that it does move. The overwhelming consensus amongst researchers is that there exists a pulsatile, cardiac dependent motion that causes both the movement of the cerebral blood and the CSF. The motion also has a respiratory component making the velocity and displacement dependent upon more than one frequency. It has also been proposed that the CSF has its own non-cardiac pulsations, which potentially adds a third frequency to understanding the motion. [33]

Quantifying brain motion has become a significant issue in the application of the TDP. The benefit to using the TDP as opposed to other perfusion measurement techniques, is that it offers continuous, real-time quantifications of tissue perfusion. Yet, with applications to the brain, clinical perfusion data recorded by the TDP has frequently shown an artifact that correlates with motion of the brain. Currently, the thermal based algorithms of the TDP do not compensate for the physical motion of brain tissue relative to the relatively stationary probe. The relative motion generally adds to the acquired power-time output data, creating an underlying pulsatile motion artifact leading to somewhat elevated perfusion readings. In order to get the most accurate perfusion results, it is imperative to have a model that correctly considers all elements of the thermal diffusion environment. It is advantageous that brain motion has been studied extensively in the MR literature. It is also very promising that researchers have proposed mathematical models that have accurately depicted blood flow and CSF flow. This extensive literature provides a strong base of data from which to construct an enhanced thermal model that compensates for relative brain-tissue motion on the sensor.

The TDP measures local tissue perfusion. It is implanted in the brain, and often attached firmly to the skull by a bolt. When the brain moves, the probe may or may not move with the moving brain tissue. Between the skull and the brain tissue, is the subarachnoid space. The catheter shaft of the probe transverses this region. If there is a high flowing CSF velocity traveling orthogonal to the probe shaft, it could also conceivably induce another small motion. Therefore if the probe penetrates the skull perpendicularly straight into the brain, the probe will experience forces that are moving up and down with the

brain tissue and side to side with the oscillating CSF. The forces actuality depends upon the angle of implantation. It is important to note that there are more than one component to the induced motion artifact.

In clinical applications, the probe will be implanted in and terminated in one of the cerebral lobes. The magnitude of the motion in the brain stem and spinal cord is intense in comparison to the motion of the cerebral lobes. The cerebral lobes have different overall velocities, as determined by Enzmann et al., [18] and Poncelet et al. [19]. Enzmann recorded velocities below 1.5mm/sec and displacements lower than 0.1mm. The smallest displacement was in the pariental lobe, which is at the top, back of the head. According to Enzmann et al., the pariental lobe moves with approximately half the velocity and half the displacement. This information might provide useful when determining a location to implant the probe. Of course, the ultimate location for placing the probe is based on the specific clinical indication.

Poncelet et al. [19] studied brain parenchymal, which corresponds to the bulk tissue in the brain, the neurons. In examining motion, it was established that the deep gray matter moves with a higher velocity. Thus, it can be postulated that increased brain depth corresponds with increased brain velocity. Poncelet also reported that the highest velocities are seen in the cephalocaudal (head-tail) direction. Velocity is significantly less in the mediolateral (middle to outside) and anteroposterior (front to back). Nonetheless, the lobes, deep gray matter, and corpus callosum, exhibit motion in all three

planes of space. It is important for clinical applications of the TDP to acknowledge that, even though they are at different strengths, there is going to be a 3-D motion.

To apply the information found in the literature research to the TDP system, clinical data analysis is going to be necessary. The most accurate way to figure out a trend is to minimize the variables. This means that when evaluating clinical perfusion data, it will be good to consider data taken from the same location of the brain to eliminate location dependent velocity and displacement.

6.4 Recommendations and Suggestions for Future Works

In summary, this thesis deals with two TDP/MR issues. First, the effect of the EM fields on the operation of the TDP sensor itself and potential patient safety issues from EM field heating (joule heating) of the sensor and its leads. Second, the effect of the TDP probe on MR image blurring. Compounding each is the affect of brain motion on both the quality of TDP perfusion value, as well as, the MR image. To minimize these affects the following recommendations are offered:

Effect of EM field on TDP operation:

1. Consider alternating TDP perfusion measurements, the MR scan, and then resuming TDP measurements. Thus eliminating active TDP data acquisition during scanning.

2. Use lead wires of low resistance, and thin dieameter. This will help reduce MR induced eddy currents and Joule heating, which can result in sensor heating.

3. Use twisted lead wire pairs to cancel out the effect of induced currents and induced magnetic fields.

4. Seek thermistor material compositions that reduce susceptibility effects.

Effect of TDP on MR image quality:

1. Reduce the size of the sensor compatible with TDP perfusion sensitivity.

2. Use low resistance lead wires of small size in both length and diameter.

3. Use MR compatible materials with a susceptibility close to that of the tissue.

Effect of brain motion on TDP measurement:

1. Know which parts of the brain move.

2. Know the displacement and velocity of motion as a function of location within the brain.

3. Seek to avoid relative probe-tissue motion by appropriate probe positioning within the brain and the depth of probe placement.

4. Characterize effects of probe-tissue motion on the probe power-time relationship. The probe-power time relationship determines the most motion induced artifact in the measured TDP perfusion value.

5. Using the data of 4., develop complementary algorithms to remove the motion artifact of the perfusion calibration.

References:

Chapter 1:
[1] Martin, G.T., Bowman, H.F. (2000) Validation of real-time continuous perfusion measurement. *Medical and Biological Engineering and Computing.* 38: 319-325.

Chapter 2:

[2] Petrella, J. and J. Provenzale. "MR Perfusion Imaging of the Brain: Techniques and Applications. American Journal of Roentgenology, Dec. 15, 1999. http://www.ajronline.org/

[3] Latchaw R, et al. "Guidelines and Recommendations for Perfusion Imaging in Cerebral Ischemia." American Heart Association Scientific Statement. http://www.strokeaha.org/

[4] Heiken, J. and J. Brown. Manual of Clinical Magnetic Resonance Imaging. Raven Press, New York. 1991.

[5] Cho, Z.; J. Jones; and M. Singh. Foundations of Medical Imaging. John Wiley and Sons, Irvine, CA. 1993.

[6] Kim et al. "Multi-slice Perfusion-based Functional MRI using the FAIR Technique: Comparison of CBF and BOLD effects", *NMR in Biomedicine,* **10**: 191-196, 1997.

[7] Ogawa, S., Tank, D.W., Menon, R., Ellermann, J.M., Kim, S.-G., Merkle, H. and Ugurbil, K. "Intrinsic Signal Changes Accompanying Sensory Stimulation: Functional Brain Mapping with Magnetic Resonance Imaging", *Proc. Natl. Acad. Sci.* USA, 89: 5951-5955, 1992

[8] Zientara, Greg. "Fast Imaging Techniques for Interventional MRI."Harvard Medical School and Brigham and Women's Hospital, Department of Radiology. Online. http://www.spl.harvard.edu:8000/pages/papers/zientara/fast/fastimaging.html

[9] P. Vajkoczy, H. Roth, P. Horn, T. Luecke, C. Thomé, U. Huebner, G.T. Martin, C. Zappletal, E. Klar, L. Schilling, P. Schmiedek, "Continuous monitoring of regional cerebral blood flow-experimental and clinical validation of a novel thermal diffusion microprobe" Journal of Neurosurgery, 93:265-274, August 2000.

Chapter 3:

[10] Shiminzu, K., T. Matsuda, T Sakurai, A. Fujita, H. Ohara, S. Okamura, S. Hashimoto, H. Mano, C. Kawai, & M. Kiri. "Visualization of Moving Fluid: Quantitative Analysis of Blood Flow Velocity Using MR Imaging." *Cardiovascular Radiology*, 1985 159:195-199.

[11] Applegate, G., F.L. Thaete, S. Meyers, P. Davis, S.L. Talagala, M. Recht, P. Wozney, & E. Kanal. "Blood Flow in the Portal Vein: Velocity Quantitation with Phase-Contrast MR Angiography. *Radiology* 1993; 187:253-256.

Chapter 4:

[14] Purves, D., G. Augustine, D. Fitzpatrick, W. Hall, A.S. LaMantia, J. McNamara, & S.M. Williams. Neuroscience, Second Edition. Sinauer Associates, Inc. 2001.

[15] Costanzo, L. Physiology, ed. 2. Saunders, New York, 2002.

[16] Nolte, John. The Human Brain: An Introduction to Its Functional Anatomy, 5th ed. Mosby, Inc. 2002

[17] Greitz, D., R. Wirestam, A. Franck, B. Nordell, C. Thomsen, & F. Stahlberg. "Pulsatile brain movement and associated hydrodynamics studied by magnetic resonance phase imaging; The Monro-Kellie doctrine revisited." *Neuroradiology* (1992) 34: 370-380.

[18] Enzmann, D. & N. Pelc. "Brain Motion: Measurement with Phase-Contrast MR Imaging" Radiology, 1992; 185: 653-660.

[19] Poncelet, B., V. Weeden, R. Weisskoff, & M. Cohen. "Brain Parenchyma Motion: Measurement with Cine Echo-Planar MR Imaging." Radiology, 1992; 185: 645-651.

[20] Maier, S., C. Hardy, & R. Jolesz. "Brain and Cerebrospinal Fluid Motion: Real-Time Quantification with M-Mode MR Imaging." *Radiology* 1994; 193: 477-483.

[21] Greitz, Dan. "Radiological assessment of hydrocephalus: new theories and implications for therapy" *Neurosurgical Review* 2004; 27: 145- 165

[22] Mokri, Bahram. "The Monro-Kellie Hypothesis: Applications in CSF volume depletion." *Neurology* 2001; 56:1746-1748

[23] Baledent O, Henry-Feugeas MC, & Idy-Perretti I. (2001) Cerebrospinal Fluid
Dynamics and Relation with Blood Flow; A Magnetic Resonance Study with
Semiautomated Cerebrospinal Fluid Segmentation. *Investigative Radiology* 36; 7,
368-377

[24] The complete 20th U.S. edition of Gray's *Anatomy of the Human Body*, published in
1918, the content of which is in the public domain. http://www.bartleby.com/107/

[25] BrainInfo (2007), Neuroscience Division, National Primate Research Center,
University of Washington, http://www.braininfo.org.

[26] "Anatomical terms of location." *Wikipedia, The Free Encyclopedia*. Wikimedia
Foundation, Inc. Jan 2007
<http://en.wikipedia.org/w/index.php?title=Anatomical_terms_of_location&oldid
=101456105>.

[27] Egnor, M., A. Rosiello, & L. Zheng. "A Model of Intracranial Pulsations" *Pediatric
Neurosurgery*. 2001, 35: 284-298.

[28] Egnor, M., L. Zheng, A. Rosiello, F. Gutman, & R. Davis. "A Model of Pulsations
in Communicating Hydrocephalus" *Pediatric Neurosurgery*. 2002, 36: 281-303.

[29] Wagshul, M., J. Chen, M. Egnor, E. McCormack, & P. Roche. "Amplitude and
phase of cerebrospinal fluid pulsations: experimental studies and review of the
literature." *Journal of Neurosurgery,* 2006, 104:810-819.

[30] Linninger, A., C. Tsakiris, D. Zhu, M. Xenos, P. Roycewicz, Z. Danziger, & R.
Penn. "Pulsatile Cerebrospinal Fluid Dynamics in the Human Brain" *IEEE
Transactions on Biomedical Engineering*, 2005. Vol. 52;4:557-565.

[31] Nitz, W., W. Bradley, A. Watanabe, R. Lee, B. Burgoyne, R. O'Sullivan, & M.
Herbst. "Flow Dynamics of Cerebrospinal Fluid: Assessment with Phase-Contrast
Velocity MR Imaging Performed with Retrospective Cardiac Gating" Radiology,
1992; 183:395-405.

[32] Alperin, N., E. Vikingstad, B. Gomez-Anson, & D. Levin. "Hemodynamically
Independent Analysis of Cerebrospinal Fluid and Brain Motion Observed with
Dynamic Phase Contrast MRI." *Magnetic Resonance Medicine* 1996; 35:741-754.

[33] Davidson, H., K. Welch, & M. Segal, Physiology and pathophysiology of the
cerebrospinal fluid. Churchill Livingstone, New York; 1987.

[34] "A Primer on Medical Device Interactions with Magnetic Resonacne Imaging
Systems" US Department of Health and Human Services, The Food and Drug

Administration; Center for Device and Radiological Health. Released Feb. 7, 1997. http://www.fda.gov/cdrh/ode/primerf6.html

[35] Levy, L.M. & G. Di Chiro. "MR phase imaging and cerebrospinal fluid flow in the head and spine." Neuroradiology 1990; 32:399-406.

[36] Goldman, R., J. Stern, J. Engel, & M. Cohen. "Acquiring simultaneous EEG and functional MRI" Clinical Neurophysiology 2000; 111: 1974-1980.

Chapter 5:

[40] Schenck, John F. "The role of magnetic susceptibility in magnetic resonance imaging: MRI magnetic compatibility of the first and second kinds." *Med. Physics* 1996 (6); 23: 815-850.

[41] Shellock, Frank G. "Metallic Surgical Instruments for Interventional MRI Procedures: Evaluation of MR Safety." *Journal of Magnetic Resonance Imaging* 2001; 13:152-157.

[42] Schueler, BA; Parrish, TB; Lin, JL, Hammer, BE; Pangrle, BJ; Riternour, ER; Kucharczyk, J; and Trutwit, CL. "MRI Compatibility and Visibility Assessment of Implantable Medical Devices." *Journal of Magnetic Resonance Imaging* 1999; 9:596-603.

[43] O'Handley, Robert C. *Modern Magnetic Materials.* Wiley, New York. 2000.

[44] Roguin, M.M. Zviman, G.R. Meininger; E.R. Rodrigues; T.M. Dickfeld; D.A. Bluemke, A. Lardo, R.D. Berger, H. Calkins, and H.R. Halperin. "Modern Pacemaker and Implantable Cardioverter/Defibrillator Systems Can Be Magnetic Resonance Imaging Safe: In Vitro and In Vivo Assessment of Safety and Function at 1.5T." *Circulation* 2004;110:475-482.

[45] Hopper, T., B. Vasilic, J. Pope, C. Jones, C. Epstein, H.K. Song, & F. Wehrli. "Experimental and computational analyses of the effects of slice distortion from a metallic sphere in an MRI phantom" *Magnetic Resonance Imaging* 2006; 24: 1077-1085.

[46] Bennett, L.H., P.S. Wang, & M.J. Donahue. "Artifacts in Magnetic Resonance Imaging From Metals," *American Institute of Physics* 1996; [S0021-8979(96)49808-4]

[47] Yeung, C. J., R. Susil, & E. Atalar (2002). "RF Safety of Wires in Interventional MRI:Using a Safety Index" *Magnetic Resonance in Medicine* 2002; 47:187–193.

[48] Graf. H., U. Lauer, & F. Schick. "Eddy-Current Induction in Extended Metallic Parts As a Source of Considerable Torsional Moment." Journal of Magnetic Resonance Imaging 2006; 23:585-590.

[49] Schiffer, P., A.P. Ramirez & S.W. Cheong "Low Temperature Magnetoresistance and the Magnetic Phase Diagram of $La_{1-x}Ca_xMnO_3$" *Physical Review Letters* 1995; Vol 75; 18:3336-3339. Copyright (1995) by the American Physical Society.

[50] Muller-Bierl, Bernd, H. Graf, U. Lauer, G Steidle, & F. Schick. "Numerical modeling of needle tip artifacts in MR gradient echo imaging" *Medical Physics* 2004; 31"579-587.

[51] Grigoryan, L., M. Furusawa, H. Hori, & M. Tokumoto. "Large magnetoresistance in intercalated Cu oxides." *Physical Review* 1997; 56;21:13720-13723.